Identification and Improvements of an Automotive Diesel Engine Model purposed for Model Based Diagnosis

Sven Öberg

7th December 2001

Identification and Improvements of an Automotive Diesel Engine Model purposed for Model Based Diagnosis

Master's thesis

performed in **Vehicular Systems**,
Dept. of Electrical Engineering
at **Linköpings Universitet**

Performed for **DaimlerChrysler AG**

by **Sven Öberg**

Reg nr: LiTH-ISY-EX-3161

Supervisors: **Dr. Mattias Nyberg**
Linköpings Universitet
Thomas Stutte
DaimlerChrysler AG

Examiner: **Dr. Lars Eriksson**
Linköpings Universitet

Linköping, 7th December 2001

Avdelning, Institution Division, Department Vehicular Systems, Dept. of Electrical Engineering		**Datum** Date 7th December 2001

Titel	Identifiering och förbättring av en dieselmotormodell vars ändamål är modellbaserad diagnos
Title	Identification and Improvements of an Automotive Diesel Engine Model purposed for Model Based Diagnosis
Författare Author	Sven Öberg

Sammanfattning
Abstract

The objective in this thesis is to improve a previously developed model for an automotive diesel engine equipped with EGR and VNT. The engine is the Mercedes-Benz OM611, 2.2 liter four cylinder turbocharged diesel engine. The engine is fitted in a research car along with a measurement system and measurements with this system are used both for modeling and validation.

The valve of the EGR system was changed and the main task was to make a model for the new valve. But the performance of an EGR system model is dependent of the overall performance of the engine model. Therefore the entire engine model will be considered, attempting to make improvements in different subsystems. Finally the model of the EGR system will be added to this. The results show that the final model agree well with measurement data and it is shown that the main errors are caused by the models of exhaust manifold and turbo.

The model is purposed to be used in a model based diagnostics system. The resulting model is therefore tested in a simple diagnostics system for intake manifold leakage. The results show that the model allows for detection of a 4 mm diameter hole in the intake manifold.

Abstract

The objective in this thesis is to improve a previously developed model for an automotive diesel engine equipped with EGR and VNT. The engine is the Mercedes-Benz OM611, 2.2 liter four cylinder turbocharged diesel engine. The engine is fitted in a research car along with a measurement system and measurements with this system are used both for modeling and validation.

The valve of the EGR system was changed and the main task was to make a model for the new valve. But the performance of an EGR system model is dependent of the overall performance of the engine model. Therefore the entire engine model will be considered, attempting to make improvements in different subsystems. Finally the model of the EGR system will be added to this. The results show that the final model agree well with measurement data and it is shown that the main errors are caused by the models of exhaust manifold and turbo.

The model is purposed to be used in a model based diagnostics system. The resulting model is therefore tested in a simple diagnostics system for intake manifold leakage. The results show that the model allows for detection of a 4 mm diameter hole in the intake manifold.

Keywords: Identification, Exhaust Gas Recirculation, Diesel, Variable Nozzle Turbine, Volumetric Efficiency, Fault Diagnosis

Preface

The outline of this thesis is divided into chapters as described in the following paragraphs.

Chapter 1, Introduction: An introduction to this thesis.

Chapter 2, Turbocharged Diesel Engines: A brief introduction to turbocharged diesel engines, especially to the Mercedes-Benz OM611 engine and it's Exhaust Gas Recirculation (EGR) and Variable Nozzle Turbine (VNT) features.

Chapter 3, Measurement Setup: Overview of the measurement system in the research car.

Chapter 4, Engine Model: Description of the engine model used and the extensions made to the pumping and turbo submodels.

Chapter 5, EGR Model: Description of how the EGR model has been developed.

Chapter 6, Validation: Validation of extensions made to the model and also a complete validation of the entire model for different driving conditions, both with and without EGR.

Chapter 7, Diagnosis: Implementation of the EGR model in a simple diagnostics system.

Chapter 8, Summary, Conclusions and Extensions: Discussion about the conclusions, that can be drawn from this thesis, a procedure summary and a list of possible future extensions to this work.

Work on the same research car and measurement setup has already been performed in [1, 2, 3]. Therefore in principal entire Chapter 2 and 3 are, under permission, taken from [1] except for Section 3.5.

Acknowledgments

<div align="right">

Linköping, December 2001
Sven Öberg

</div>

Notation

Nomenclature

Symbol	Quantity	Unit
A_{EGRV}	Effective area of EGR valve opening	m^2
$\hat{A}_{EGRV}$	Estimated effective area of EGR valve opening	m^2
c_p	Specific heat capacity at constant pressure	$J/(kg \cdot K)$
$c_{p,Intake}$	Intake manifold specific heat capacity at constant pressure	$J/(kg \cdot K)$
$c_{p,Air}$	Air specific heat capacity at constant pressure	$J/(kg \cdot K)$
$c_{p,Exh}$	Exhaust gas specific heat capacity at constant pressure	$J/(kg \cdot K)$
$c_{v,Intake}$	Intake manifold specific heat capacity at constant volume	$J/(kg \cdot K)$
$c_{v,Air}$	Air specific heat capacity at constant volume	$J/(kg \cdot K)$
$c_{v,Exh}$	Exhaust gas specific heat capacity at constant volume	$J/(kg \cdot K)$
C_D	Discharge coefficient	-
e_{max}	Maximum error	%
e_{mean}	Mean error	%
e_{RMS}	Root mean square error	%
h_{HT}	Heat transfer coefficient	W/K
$\dot{H}$	Change of enthalpy	J/s
l_{VNT}	VNT lever position	mm
$\hat{l}_{VNT}$	Estimated VNT lever position	mm
m_{Air}	Mass of air in intake manifold	kg
m_{EGR}	Mass of exhaust gas in intake manifold	kg
m_{Exh}	Mass of exhaust gas in exhaust manifold	kg
$\dot{m}_{Air}$	Change of air mass in intake manifold	kg/s
$\dot{m}_{EGR}$	Change of exhaust gas mass in intake manifold	kg/s
$\dot{m}_{Exh}$	Change of exhaust gas mass in exhaust manifold	kg/s
$\dot{m}_{Intake}$	Change of total gas mass in intake manifold	kg/s
$\dot{m}_{Reservoir}$	Change of total gas mass in reservoir	kg/s

Symbol	Quantity	Unit
N_{Eng}	Engine speed	RPM
p_{Amb}	Ambient pressure	Pa
p_{Exh}	Exhaust manifold pressure	Pa
p_{Intake}	Intake manifold pressure	Pa
p_{Turb}	Pressure after turbine	Pa
$\dot{p}_{Intake}$	Change of intake manifold pressure	Pa/s
$\dot{q}_{Intake}$	Rate of heat transfer in the intake manifold	J/s
Q_{LHV}	Fuel lower heating value	J/kg
R_{Intake}	Gas constant for intake manifold gas mix	$J/(kg \cdot K)$
R_{Air}	Gas constant for air	$J/(kg \cdot K)$
R_{Exh}	Gas constant for exhaust gas	$J/(kg \cdot K)$
X_{EGRV}	EGR valve control-signal	$\%$
X_{Inj}	Fuel injection control-signal	$\%$
X_{VNT}	VNT control-signal	$\%$
T_{Amb}	Ambient temperature	K
T_{EGR}	Temperature of EGR flow into intake manifold	K
T_{EGRV}	Temperature of EGR flow after EGR valve	K
T_{Exh}	Exhaust manifold temperature	K
T_{Intake}	Intake manifold temperature	K
T_{Inter}	Temperature after intercooler	K
T_{Oil}	Oil temperature	K
T_{Turb}	Temperature after turbine	K
T_{Wall}	Intake manifold wall temperature	K
T_{Water}	Cooling water temperature	K
$\dot{T}_{Intake}$	Change of intake manifold temperature	K/s
V_{Exh}	Exhaust manifold volume	m^3
V_{Eng}	Displaced volume	m^3
V_{Intake}	Intake manifold volume	m^3
W_{EGR}	Mass-flow through EGR pipe	kg/s
W_{Exh}	Mass-flow into exhaust manifold	kg/s
W_{Fuel}	Mass-flow of fuel into cylinders	kg/s
W_{Inlet}	Mass-flow into cylinders	kg/s
W_{Inter}	Mass-flow after intercooler	kg/s
$W_{Restriction}$	Mass-flow through restriction	kg/s
W_{Turb}	Mass-flow through turbine	kg/s
$\gamma = c_p/c_v$	Ratio of heat capacities	-
ϵ_{EGRC}	EGR cooler efficiency	-
η_{Vol}	Volumetric Efficiency	-
ρ_{Intake}	Intake manifold density	kg/m^3
ρ_{Inlet}	Density at inlet port	kg/m^3

Abbreviations

Abbreviation	Explanation
CDI	Common rail Direct Injection
CI	Compression Ignited
ECU	Electronic Control Unit
EGR	Exhaust Gas Recirculation
MVEM	Mean Value Engine Model
NOx	Nitrogen-oxide
OBD	On Board Diagnostics
RPM	Revolutions Per Minute (engine speed)
RMS	Root Mean Square (error)
SI	Spark Ignited
VNT	Variable Nozzle Turbine
VGT	Variable Geometry Turbocharger

x

Contents

Chapter 1

Introduction

This master's thesis has been performed for DaimlerChrysler AG [4], Research and Technology (FT2/EA). DaimlerChrysler is one of the worlds largest automotive producers owning brands like Mercedez-Benz, Chrysler, Smart and Freightliner.

1.1 Background

The emission requirements on automotive engines have over the years become more and more strict. In order to keep up with new legislative regulations, more and more complex solutions are implemented. Thereby the possibility of malfunctions increase. Since the year 2000, all cars sold in EU must be equipped with an on-board diagnostics (OBD) system [3]. The purpose of such a system is to make sure, that the requirements on emissions are kept, not only when the car is new but also later. The aim is, that when a fault that will increase emissions appear, it should be detected. Faults would typically be due to wear or malfunction. An example of how a fault could influence emissions is if a leakage occur on the engine air intake path. Less air than expected would then go into the cylinders but fuel injection could be unaffected and emissions would then be influenced.

One way to construct a diagnosis system is to utilize model based diagnosis. This approach is, as the name implies, based on having a model of the engine and then on-line compare the output from the model with signals measured on the engine. The better the model is, the better the diagnostics system will perform. In this thesis concentration will be on the construction of this model.

1.2   Objectives

Work has already been put into developing a model of the particular engine, that will be looked at in this thesis [3,1]. The results have been fairly good except for when the EGR system (see Section 2.2) is turned on. This is one of the conclusions in [1].

The objective in this thesis is to improve the previously developed model. The valve of the EGR system was changed and the main task was to make a model for the new valve. But the performance of an EGR system model is dependent on the overall performance of the engine model. The reason for this is, that the EGR system constitutes a feedback loop in the air-path system. Therefore the entire engine model will be considered, attempting to make improvements in different subsystems. Finally the model of the EGR system will be added to this.

1.3   Method

The model has been developed in a Matlab/Simulink environment. Modeling and validation are then made using measurements from a measurement system installed in a research car. For modeling are ten minutes long measurements used. From those measurements are identifications made. Identification measurements are made during mixed city- and highway driving. For validation are five minutes long measurements made during mixed, highway and uphill driving used. The data used for validation is not the same as that used for identification so that a proper validation can be made.

1.4   Target Group

This master thesis is aimed for undergraduate or graduate engineers with basic knowledge in vehicular systems.

Chapter 2

Turbocharged Diesel Engines

This chapter describes how turbocharged diesel engines work and in particular the engine in the research car of this project, the Mercedes-Benz OM611 engine. Work on this project have already been performed as described in [1, 2, 3] and therefore in principle this entire chapter is, under permission, taken from [1]. The information about turbocharged diesel engines presented in this chapter, and much more, can be found in [5, 6, 7]

Diesel engines, also known as Compression Ignition (CI) engines, have been turbocharged for more than five decades. It is the operating principle of the CI engine that enables them to be turbocharged without some of the problems occurring when turbocharging Spark Ignition (SI) engines. The basic idea of turbocharging is to increase the amount of air inducted in the cylinders. The more air inducted, the more fuel can be injected, and the more power output is obtained. A turbocharged engine can then be made smaller than a naturally aspirated engine which has the same power output, i.e. a turbocharged engine has a higher power to weight ratio. In a turbo system a turbine-compressor combination, powered by energy from the exhaust gases is used to boost the intake air pressure. Another possibility is to compress the air with a mechanically driven pump.

In a diesel engine, the fuel is injected directly into the cylinder. Before the fuel is injected, air is inducted and compressed in the cylinder. During compression the temperature is increased to over the self ignition temperature of the fuel. When combustion is required to start the fuel is injected, and after a small delay period when the liquid fuel evaporates and mixes with air, spontaneous ignition occurs. Since combustion starts before the whole amount of fuel is injected the possibility

for negative effects such as knock is limited.

The operating principle of a four stroke CI-engine can be described in the following way. In Figure 2.1 the movement of the piston and the valves are shown for the four strokes.

Intake stroke The intake valves are open and as the piston moves downwards the cylinder is filled with fresh air.

Compression stroke The intake valves closes and as the piston moves upwards the air in the cylinder is compressed. This causes the temperature to rise to about 800 K. In the end of this stroke the fuel is injected. The air temperature and pressure are above the fuels ignition point, therefore spontaneous ignition initiates the combustion process.

Expansion stroke Due to the high pressure created by the combustion the piston is accelerated downwards. In the end the exhaust valves open.

Exhaust stroke The piston moves upwards and pushes the burned gases into the exhaust system. When the piston reaches its top position a new cycle starts.
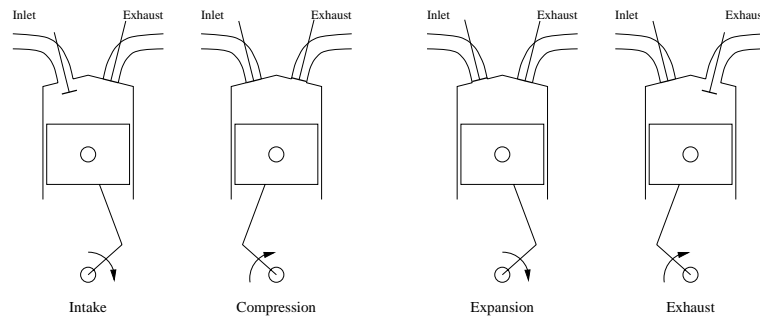
Figure 2.1: The four strokes of an internal combustion engine.

2.1   The OM611 engine

The engine that is modeled in this master thesis is the Mercedes-Benz OM611. This is a 2.2 liter, 16 valve, four cylinder diesel engine with common rail direct injection (CDI) fitted in a Mercedes E-class. More information on the OM611 engine can be found in [8]. A schematic overview of the engine is given in Figure 2.2. The engine has no throttle and is equipped with both Exhaust Gas Recirculation (EGR) and Variable Nozzle Turbine turbocharger (VNT). EGR and VNT will be described in the following sections.

Figure 2.2: Schematic overview of the OM611 engine.

2.2 Exhaust Gas Recirculation

The concept of EGR has been introduced as a way to decrease NO_x production. Since NO_x is mainly produced under high pressures and high temperatures, it is possible to control its formation, by either reducing the compression or the temperature in the combustion chamber. When using EGR, i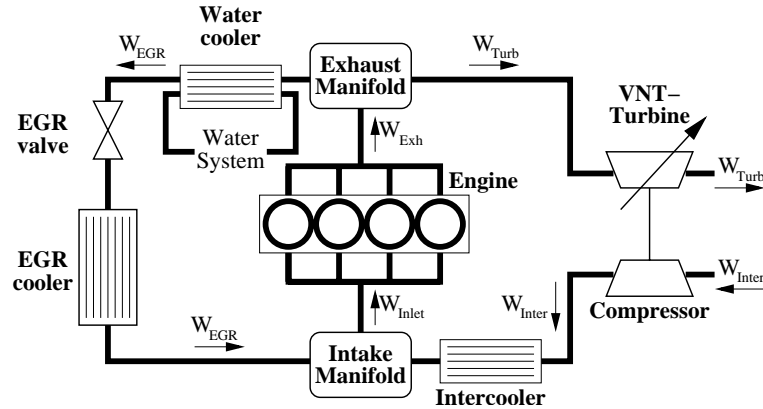t is mainly the maximum combustion temperature that is affected. EGR mixes cooled exhaust gas, burned gases, into the intake air stream. This helps to lower the maximum combustion temperatures because the burned gases dilute the normal, unburned gases that are ready for combustion.

One of the drawbacks with EGR is that it decreases the combustion stability. Because you don't want to loose driveability, i.e. power output, EGR is only active during low load conditions. The amount of EGR diesel engines can tolerate before misfire is up to 40 percent. The use of EGR reduces the formation of NO_x up to 30 percent.

2.3 Variable Nozzle Turbine Turbocharger

A conventional turbocharger has a limited optimal working area. At high engine speeds some of the flow must bypass the turbine by a waste gate, not to exceed the maximum rotational speed of the turbine. During accelerations from low engine speeds there is a time lag, called turbo lag, between the demand and the actual increase in acceleration. This lag exists because the turbine has to build up enough speed before the compressor can work effectively.

In order to widen the optimal working area, especially in the lower

engine speeds, variable nozzle turbine (VNT) turbocharging is applied. The basic idea is to have a variable inlet geometry to the turbine. This is managed by a set of vanes arranged in the path of the flow. By changing the angle of the vanes, the area of the turbine inlet changes. During low engine speeds when the flow trough the engine is small one can increase the velocity of the flow by partially closing the vanes, thus gaining turbine speed. With this setup there is also no more need for a waste gate.

In some literature, the name variable geometry turbocharger (VGT) is used.

2.4   Air Path System

In this section an overview of the air path system is given. The intake manifold is a small but important part of this system. Engine models are often based on the mass flow through the engine.

In Figure 2.3 the air path system for the OM611 engine is presented. After entering the engine through the air filter (not shown in the figure), the air is compressed by the turbocharger (compressor). In the turbocharger the temperature of the air is also increased. This is an unwanted effect because the goal of the compression is to get a higher density, so the air is then cooled in the intercooler. Since there is no throttle the flow of air then directly enters the intake manifold where it can be mixed with recirculated exhaust gases. Then the air is inducted into the cylinders where combustion takes place. On the outlet side of the cylinders, the exhaust gases enters the exhaust manifold, from where a portion of the gases can be recirculated through the EGR cooler, back to the intake manifold. The rest is led through the turbine (VNT) that drives the compressor and then through catalysts and silencer (not shown).
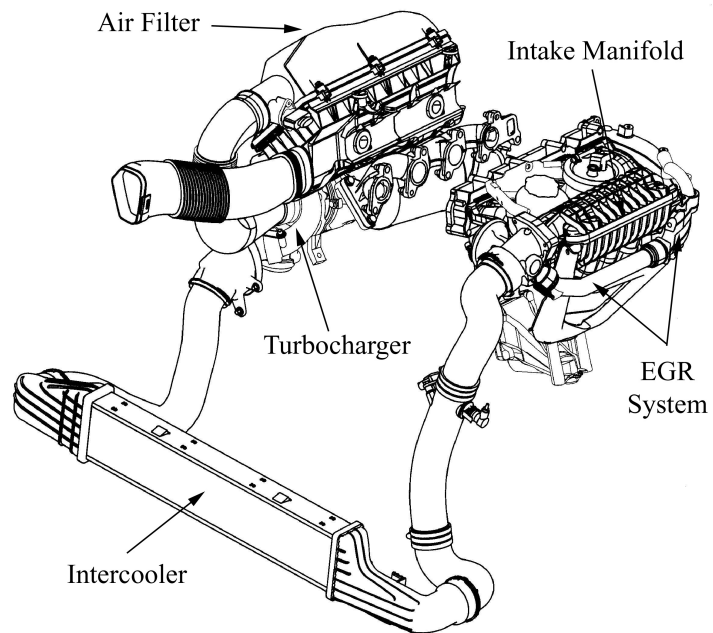
Air Filter

Intake Manifold

Turbocharger

EGR
System

Intercooler

Figure 2.3: Overview of the air path system of the Mercedes-Benz OM611 engine.

Chapter 3

Measurement Setup

This chapter describes the measurement system used in this thesis. Work on this project have already been performed as described in [1,2,3] and therefore in principle this entire chapter is, under permission, taken from [1] except from Section 3.5.

The research car is a Mercedes E-class with the 2.2 liter diesel engine described in Chapter 2. A number of extra sensors have been installed in this engine to be able to closely monitor the behavior of certain variables. The measurement system consists of five major components. An overview of them is given in Figure 3.1.

3.1   The Mac2 measuring and application unit

For measuring and storing variables from the research car a laptop computer is used. This computer has to be able to communicate with the Engine Control Unit (ECU) and the additional measuring equipment installed. To do this the Mac2 unit is used as an interface. Measuring data is gathered by the ECU and the additional sensors and sent via the Mac2 unit to the laptop. In the laptop it is stored and can be saved as a Matlab m-file. The software used for this application is called INCA and it is distributed by ETAS GmbH [9]. This software is also used for controlling the engine via the ECU and to change the programming of the ECU.
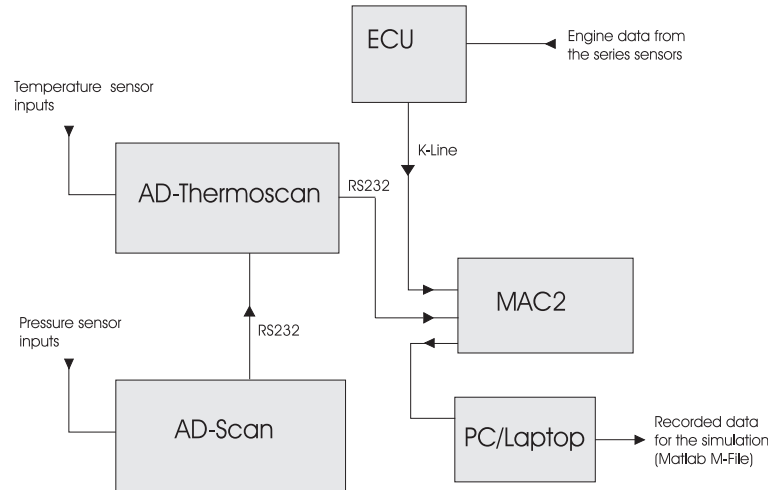
Figure 3.1: Schematic figure of the measurement components.

3.2   The engine control unit (ECU)

The standard ECU usually integrated in the OM611 engine has been
exchanged for a modified ECU. This ECU is equipped with an extra
Flash-EPROM memory. This is done to allow modifications in the
engine control program. Modifications to the control program were
done a couple of times during the work on this thesis. For example the
EGR valve had to be set in a closed position during some measurements,
and the ability to specify the amount of fuel to be injected, was used
while doing measurements on a roll testbed.

3.3   The AD-Thermoscan

The AD-Thermoscan is used for temperature measurements. It has
fourteen channels that can be connected to thermal elements, in this
case K-elements $(N_i C_r - Ni)$. The resolution of the temperature mea-
surement can be chosen between two ranges, depending on whether a
high resolution is wanted over a shorter range or a lower resolution over
a longer range. The two ranges are from -25°C to 1250°C with a reso-
lution of 5°C, or from -50°C to 205°C with a resolution of 1°C. Which
range is used depends on where the sensor is located, both ranges are
used in this measurement system. The device is produced by CSM
GmbH.

3.4 The AD-Scan

The AD-Scan is similar to the AD-Thermoscan, only it is used for pressure measurement. The pressure sensors connected to the measuring channels are so called expansion stripe elements. They transform a change of pressure to a change in resistance. The change of resistance causes a voltage change, which is what the AD-Scan handles. With this setup pressures ranging from 500 mBar to 4000 mBar can be measured.

3.5 Measured Variables

Table 3.1 presents all the variables that the measurement system can measure. The variables are sorted by measurement device.

Variable	Explanation
ECU	
t_{ECU}	ECU time vector
N_{Eng}	Engine Speed
p_{Amb}	Ambient pressure
W_{Inter}	Air mass-flow after intercooler
T_{Inter}	Temperature after intercooler
p_{Intake}	Intake manifold pressure
T_{Water}	Cooling water temperature
T_{Oil}	Oil temperature
X_{Inj}	Fuel injection control signal
X_{VNT}	VNT vane control signal
X_{EGRV}	EGR valve control signal
AD-Thermoscan	
t_{Termo}	Thermoscan time vector
T_{Amb}	Ambient temperature
T_{Filt}	Temperature after air filter
T_{Comp}	Temperature after compressor
T_{Inter}	Temperature after intercooler
T_{Intake}	Temperature in intake manifold
T_{Wall}	Temperature on wall of the intake manifold
T_{Exh}	Temperature in exhaust manifold
T_{EGR}	Temperature after EGR cooler
T_{Turb}	Temperature after turbine
T_{Cat1}	Temperature after first catalyst
T_{Cat12}	Temperature betw. first and second catalyst
T_{Cat2}	Temperature after second catalyst
AD-Scan	
t_{AD}	AD-Scan time vector
p_{Filt}	Pressure after air filter
p_{Comp}	Pressure after compressor
p_{Intake}	Pressure in intake manifold
p_{Exh}	Pressure in exhaust manifold
p_{Turb}	Pressure after turbine

Table 3.1: All variables of the measurement system listed by source device.

Chapter 4

Engine Model

The aim of this thesis is to improve an existing model of the engine described in Section 2.1. It will be described in this chapter how the engine previously has been modeled and what improvements has been made in this thesis. Both the original model and the improvements made to it are presented, so a full overview of the model can be given. The ideas for what improvements should be made are mainly based on the conclusions made in [1]. The main conclusion was that the model of the EGR system is inaccurate. The work presented in this chapter is aimed to get a good model for the engine when EGR is turned off. The EGR system can then be modeled in Chapter 5, knowing that the model of the engine as a whole is good enough to be used as basis for the EGR system. The basis for the modeling work is measurements, made using the measurement system described in Chapter 3. The measurements used for modeling are, in most cases, ten minutes long and have been made during mixed city and highway driving. Different measurements made using the very same measurement system, will be used in Chapter 6 to validate the model presented in this chapter.

It is shown in Figure 4.1 how the model is divided into subsystems. The arrows indicate the flow of information through the model. The model inputs are all measured directly from the ECU. This means that they all are series production sensors. The goal is to make a model needing no additional sensors. There exists a series production sensor for ambient temperature but this sensor is very slow, so an additional sensor for ambient temperature has been installed. All other sensors used for inputs are series production sensors. The inputs are all described in Table 4.1. This chapter deals with the Intake, Pumping, Combustion, Exhaust and Turbo subsystems. Each of these systems will be described in the following sections in this chapter whereas the EGR system is modeled separately in Chapter 5.

The model is a lumped parameter, mean value engine model (MVEM).

Input	Explanation
N_{Eng}	Engine Speed
W_{Inter}	Air mass-flow after intercooler
T_{Inter}	Temperature after intercooler
T_{Oil}	Oil temperature
T_{Amb}	Ambient temperature
p_{Amb}	Ambient pressure
X_{EGRV}	EGR valve control signal
X_{Inj}	Fuel injection control signal
X_{VNT}	VNT vane control signal

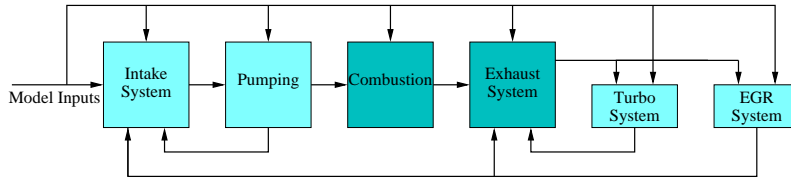Table 4.1: Inputs to the engine model.

Figure 4.1: Overview of the subsystem build-up in the engine model. Subsystems where no work has been done in this thesis are shadowed.

MVEM means that no variations within cycles are covered by the model and makes the model valid only for time intervals far greater than one engine cycle [5]. The model is based on quasi steady-state flow assumptions and it combines physical principles, with the use of steady state maps. The model covers the entire engine, starting after the air intake compressor and ending at the exhaust turbine. Three or four states are used to model the engine. They are presented in Table 4.2. Two different setups of intake manifold states have been used previously in this model (see Section 4.1). First pressure and mass (both air- and EGR mass) and then pressure and temperature. A mass state in the exhaust manifold is then added to this. All modeling is kept as simple as possible to allow for fast computations. The model has been implemented in Matlab/Simulink.

4.1 Intake Manifold Model

The engine model has previously been used with two different intake manifold models. It is necessary to compare them so that the best can be chosen as basis for the work in the following sections. The models

State	Model 1	Model 2	Explanation
$\dot{p}_{Intake}$	X	X	Change of pressure in intake
$\dot{m}_{Air}$	X		Change of air mass in intake
$\dot{m}_{EGR}$	X		Change of EGR gas mass in intake
$\dot{T}_{Intake}$		X	Change of temperature in intake
$\dot{m}_{Exh}$	X	X	Change of exhaust gas mass in exh.

Table 4.2: Different states in the engine model.

are presented below and then the simulation results are compared in Section 6.1. The model used originally [3] was a pressure and mass state model with adiabatic assumption, i.e. with no heat transfer from the intake manifold. The intake manifold state equations are then:

$$\dot{p}_{Intake} = \frac{1}{V_{Intake}}\left[R_{Air}\gamma_{Air}W_{Inter}T_{Inter} + \right.$$
$$+ R_{Exh}\gamma_{Exh}W_{EGR}T_{EGR} -$$
$$\left. - R_{Intake}\gamma_{Intake}W_{Inlet}T_{Intake}\right], \qquad (4.1)$$

$$\dot{m}_{Air} = W_{Inter} - \frac{m_{Air}}{m_{Air} + m_{EGR}}W_{Inlet},$$
$$\dot{m}_{EGR} = W_{EGR} - \frac{m_{EGR}}{m_{Air} + m_{EGR}}W_{Inlet} \qquad (4.2)$$

where

$$T_{Intake} = \frac{p_{Intake}V_{Intake}}{(m_{Air} + m_{EGR})R_{Intake}},$$
$$R_{Intake} = \frac{R_{Air}m_{Air} + R_{Exh}m_{EGR}}{m_{Air} + m_{EGR}},$$
$$c_{v,Intake} = \frac{c_{v,Air}m_{Air} + c_{v,Exh}m_{EGR}}{m_{Air} + m_{EGR}},$$
$$c_{p,Intake} = c_{v,Intake} + R_{Intake},$$
$$\gamma_x = c_{p,x}/c_{v,x}.$$

The pressure state, $\dot{p}_{Intake}$, is built up from change in enthalpy terms, $\dot{H} = Wc_pT$, entering and leaving the intake manifold. The entering enthalpy comes from the compressor (intercooler) and the EGR system. The exiting enthalpy goes to the cylinder inlets. The pressure state is defined from the difference between the entering and exiting enthalpy. The air mass state is defined as the difference between incoming air mass-flow in the intake manifold and air mass-flow entering the cylinder inlets. The EGR mass state is the difference between EGR gas mass-

flow entering the intake manifold and the ones flowing to the cylinder inlets.

The second intake manifold model [1] used is a pressure and temperature state model including heat transfer from the intake manifold. Temperatures in the intake manifold will vary over a wider range and reach higher values, for an engine with EGR, than for a naturally aspirated engine. It will therefore be necessary to take heat transfer into consideration. As follows:

$$
\begin{aligned}
\dot{p}_{Intake} \quad = \quad & \frac{1}{V_{Intake}}\Bigg[R_{Intake}\gamma_{Intake}W_{Inter}T_{Inter} + \\
& + R_{Intake}\gamma_{Intake}W_{EGR}T_{EGR} - \\
& - R_{Intake}\gamma_{Intake}W_{Inlet}T_{Intake} - \\
& - \frac{R_{Intake}\gamma_{Intake}h_{HT}(T_{Intake} - T_{Wall})}{c_{p,Intake}}\Bigg], \qquad (4.3)
\end{aligned}
$$

$$
\begin{aligned}
\dot{T}_{Intake} \quad = \quad & \frac{R_{Intake}T_{Intake}^2}{p_{Intake}V_{Intake}}\Bigg[(\gamma_{Intake}\frac{T_{Inter}}{T_{Intake}} - 1)W_{Inter} + \\
& + (\gamma_{Intake}\frac{T_{EGR}}{T_{Intake}} - 1)W_{EGR} - \\
& - (\gamma_{Intake} - 1)W_{Inlet} - \\
& - \frac{h_{HT}(T_{Intake} - T_{Wall})}{c_{v,Intake}T_{Intake}}\Bigg], \qquad (4.4)
\end{aligned}
$$

under the assumption, that

$$
\begin{aligned}
c_{v,Intake} \quad &= \quad c_{v,Air} = c_{v,Exh}, \\
c_{p,Intake} \quad &= \quad c_{p,Air} = c_{p,Exh}, \\
R_{Intake} \quad &= \quad R_{Air} = R_{Exh}, \\
\gamma_x \quad &= \quad c_{p,x}/c_{v,x}.
\end{aligned}
$$

The pressure state equation in (4.3) is almost the same as in (4.1). The only difference is the subtracted enthalpy exiting the intake manifold through the manifold wall. The temperature state on the other hand is a bit more complicated and will not be discussed here. The derivation can be found in [1]. This model is used under the assumption, that the specific heats for air and exhaust gases are the same. Looking closer at the derivation in [1], it seems as this assumption not at all is necessary to derive the equations. However, the equations will here be used as they were implemented. $c_{p,Air}$ is 285 $J/(kg \cdot K)$ and $c_{p,Exh}$ is 287 $J/(kg \cdot K)$. So after all, the difference between specific heats for air and exhaust gases is not great.

As will be shown in Section 6.1, the heat transfer model is superior
to the adiabatic, mainly in temperature modeling but also in pressure
modeling. Having both a proper pressure and temperature model is
important, especially for the pumping model (Section 4.2).

4.1.1   Wall Temperature Model

The variable T_{Wall} introduced in (4.3) and (4.4) is the temperature on
the outside wall of the intake manifold. T_{Wall} was set manually, in the
previous use of these equations and it has not been explained exactly,
how this was done. It is therefore necessary to make a model of T_{Wall}.
There exists no series production sensor for T_{Wall} so two temperature
sensors were therefore installed in the research car. They were placed
on two separate ends of the intake manifold surface. A temperature
model will be made from the measurements of these two sensors. The
temperature on the wall was assumed to be the average of the two
sensor outputs.

The temperature on the wall of the intake manifold is probably
dependent on the temperature under the hood. The temperature under
the hood, in turn, can be seen as a function of ambient air temperature,
engine temperature and the cooling effect from the fan. However, as
the control signal for the fan was not made available, a model had to be
made up from ambient air temperature and engine temperature. There
exists a serial production sensor for the ambient air temperature, T_{Amb}
but this is too slow. So an additional sensor is used instead. A range of
sensors were tried for the engine temperature. Using a least-square fit
to the measured T_{Wall} showed, that the oil temperature sensor, T_{Oil},
on it's own was the best to describe the effect of engine temperature, on
the intake manifold wall temperature. The resulting empirical model
of the least-square fit was:

$$T_{Wall} = T_{Amb} \cdot 0.77 + T_{Oil} \cdot 0.27. \tag{4.5}$$

4.2   Pumping Model

To model the pumping of an *ideal* four stroke engine, one could say
that the average air displaced is:

$$W_{Inlet} = \frac{N_{Eng}\rho_{Inlet}V_{Eng}}{120}, \tag{4.6}$$

where 120, represents having a four stroke cycle, i.e. air is inducted
only every other revolution. It is also a unit conversion of N_{Eng}. Equa-
tion (4.6) represents the ideal case. However, the inlet port and inlet
valve restricts the amount of air inducted. It is therefore necessary to

define how efficient the induction process is. This is generally referred to as *volumetric efficiency* [5]. It is defined as, the volume flow rate of air into the intake system, divided by the rate, at which volume is displaced by the piston. If the density at the inlet port ρ_{Inlet} is assumed to be equal to the density in the intake manifold ρ_{Intake}:

$$\eta_{Vol} = 120 \frac{W_{Inlet}}{N_{Eng}\rho_{Intake}V_{Eng}}. \tag{4.7}$$

If EGR is turned off, it can be assumed that the air mass-flow after the air filter, equals the air mass-flow into the inlet:

$$W_{Inlet} = W_{Inter}. \tag{4.8}$$

This, in addition to that the ideal gas law gives

$$\rho_{Intake} = \frac{p_{Intake}}{T_{Intake}R_{Air}}, \tag{4.9}$$

makes it possible to make measurements and to calculate volumetric efficiency, for different static operating points. Volumetric efficiency can be said to be affected by a range of variables. However, it is assumed that only engine speed and air density affects the amount of air inducted. Hence $\{N_{Eng}, \rho_{Intake}\}$ will constitute an operating point. Volumetric efficiency will thus be represented by a 2D look-up table.

Volumetric efficiency maps for this model, have already been dealt with in [1]. The work in this section should be seen as an extension to that work. Two different ways to improve the volumetric efficiency map will be evaluated in this thesis. They are described in the following two subsections.

4.2.1 Volumetric Efficiency Back-flow Dependency

In the compression stroke (see Chapter 2), the cylinder pressure rises, due to piston motion towards the top center position. This, together with the fact, that the inlet valve closes slightly after the start of the compression stroke, causes a back-flow of air into the intake [5]. The air is heated by the compression in the cylinder. The back-flow will possibly affect the intake manifold temperature sensor, T_{Intake}, used in the density equation (4.9), affecting the volumetric efficiency (4.7). The influence of this back-flow, will therefore be investigated by comparing two volumetric efficiency maps. One generated using a temperature sensor positioned in the intake manifold, T_{Intake} (see Figure 4.2), and one map generated using a sensor positioned between the intake manifold and the intercooler, T_{Inter}. The latter is shown in Figure 4.3.
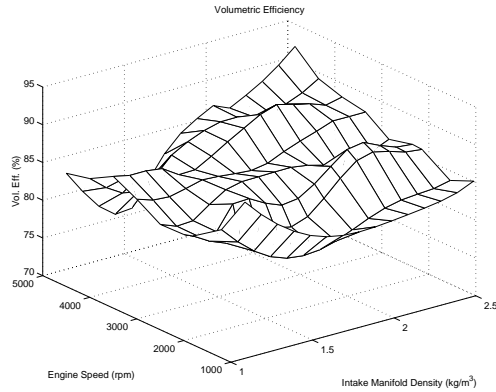
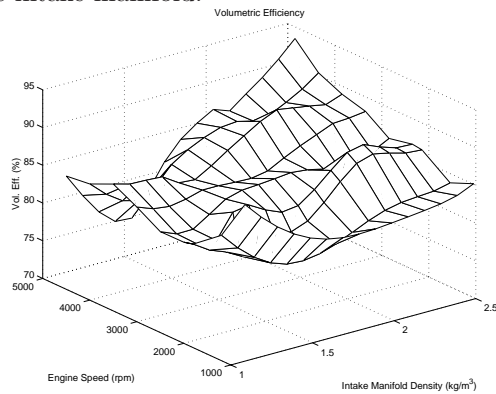Figure 4.2: Volumetric efficiency map generated using temperature sensor *inside* the intake manifold.

Figure 4.3: Volumetric efficiency map generated using temperature sensor *before* the intake manifold.

It can be seen, when Figure 4.2 and Figure 4.3 are compared, that the difference is very small. The main difference seem to be a small offset between the two plots. The plot using T_{Inter} seems to reach slightly higher values in the corners where it is extrapolated. How the difference affects the model will be validated in Section 6.2.

4.2.2   Extension to the Volumetric Efficiency map

The results in [1] show, that measurement data generated using a roll testbed for the entire car, gives better results, than using data generated using a static engine testbed.

The roll testbed data generation for the research car of this project,

had already been made and the data was still available. The data
generation had been performed by setting eight different speed mea-
surement points. Different fueling conditions were set for each of these
points, by applying different braking torques to the wheels. The fuel-
injection was controlled by a laptop communicating with the ECU, to
make the engine run statically at each measurement point. EGR was
turned off during the measurements. The idea is, that since the volu-
metric efficiency map is a function of density, it will also be accurate
for simulations, when EGR is turned on. This can be assumed since
EGR influences mainly temperature and therefore also the density.

The maximum torque that an engine can deliver decreases with
decreased engine speed. This also goes for the brake, that applies
braking torque to the wheels in the roll testbed. It was therefore only
possible to apply different torques for high engine speeds, when the
roll testbed data generation was made. For decreasing engine speeds,
less and less torque was possible. As the measurement points were
not chosen dense enough, there exists only one measurement for engine
speeds below 1800 RPM. This is at a low intake manifold density, since
the brake simply did not have power enough, at low engine speeds,
to apply high braking torques. Having measurement points for higher
density in the low engine speed area, would also be unnecessary, since
it is not part of the normal operating range of the engine, but having
only one measurement point for engine speeds below 1800 RPM, makes
interpolation (and extrapolation) in this area very inaccurate. It would
thus be necessary to increase the number of measurement points, in the
low engine speed, low density area, to get better results.

Measurements showed, that the errors at low engine speeds, caused
by the inaccurate areas in the volumetric efficiency map, were amplified
especially when EGR was turned on. Probably because a fault in W_{Inlet}
would cause a fault in the ratio $\frac{p_{Intake}}{p_{Exh}}$, that governs the amount of EGR
mass-flow, into the intake manifold (see Chapter 5). It was therefore
decided, that the volumetric efficiency map needed to be modified. Lack
of resources implied that this had to be done, without making a new
roll testbed data generation. The solution was very simple. A range of
different test-drives were made, and it was possible to manually identify
operating points with large errors, from these. Only points that seemed
fairly static were chosen. A typical length of these operating points were
3 to 15 seconds. They were then inserted into the map.

Both the original and the new set of measurement points are shown
in Figure 4.4, plotted over a typical engine performance. The mea-
surement points in the figure are non-uniformly spaced. The Matlab
function `griddata` was used to estimate a uniform grid from the data.
This function fits a surface to the in-data and then interpolates in this
surface at the points of the desired grid. `griddata` can use several meth-

ods of interpolation. Biharmonic spline interpolation is the method of interpolation used for this task. More info on this interpolation can be found in [10].

The original- and modified volumetric efficiency maps are shown in Figure 4.2 and Figure 4.5. It is obvious from comparing the two maps, that the difference is large, mainly in the low density area, where it should be. The low engine speed, high density area, has also been affected but this area has no practical use anyway, as explained above. Both the modified and the original map will be validated in Section 6.2.
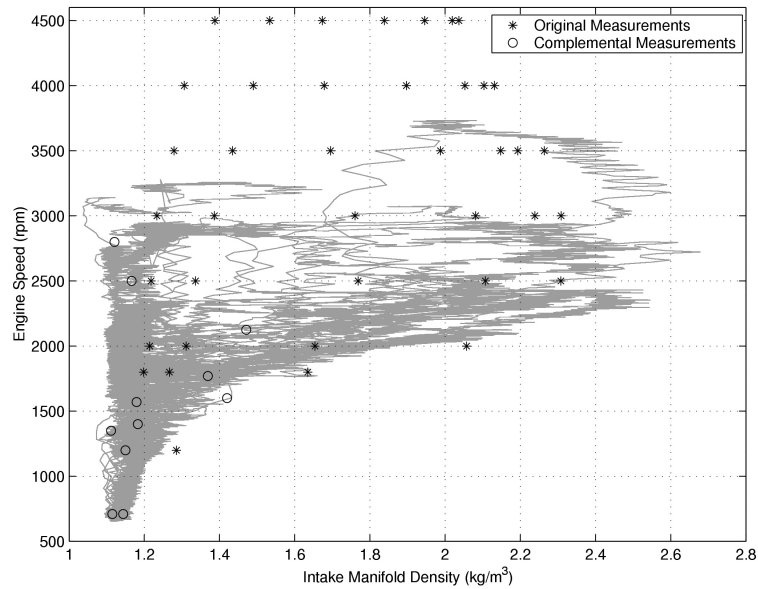

Figure 4.4: Original and complemental volumetric efficiency measurement points, plotted over a typical engine performance.

4.3 Combustion and Exhaust Model

The combustion and exhaust model, presented here, are taken from [3]. They have not been modified and appear here, only so that the entire
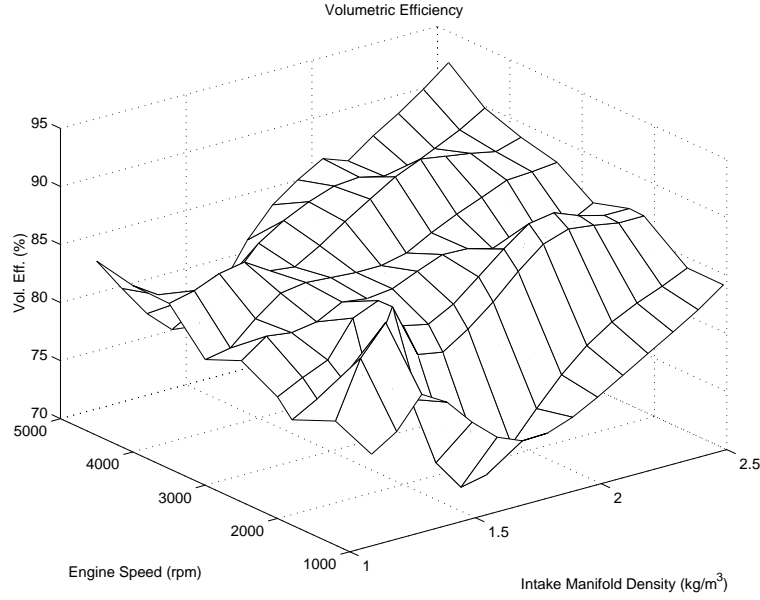
Figure 4.5: Volumetric efficiency map including additional measurement points at low engine speeds.

model can be presented. First the combustion process:

$$
\begin{aligned}
W_{Exh} &= W_{Inlet} + W_{Fuel}, \\
W_{Fuel} &= \frac{4X_{Inj}N_{Eng}}{120}, \\
T_{Exh} &= T_{Intake} + \frac{Q_{LHV}h(W_{Fuel}, N_{Eng})}{c_{p,Exh}(W_{Inlet} + W_{Fuel})}.
\end{aligned}
$$

where Q_{LHV} is the lower heating value for the fuel. $h(W_{Fuel}, N_{Eng})$ is a 2D look-up table, describing the percentage of energy put into the cylinders, that goes to heating up the exhaust gases, leaving the cylinders.

Secondly, the exhaust:

$$
\begin{aligned}
\dot{m}_{Exh} &= W_{Exh} - W_{Turb} - W_{EGR}, && (4.10) \\
p_{Exh} &= \frac{m_{Exh}R_{Exh}T_{Exh}}{V_{Exh}}. && (4.11)
\end{aligned}
$$

4.4 Turbo Model

One of the inputs to the engine model is W_{Inter} (see Table 4.1). This is the only mass-flow sensor in the engine system. Having measured mass-flow of fresh air put into the engine, means that there is no need in making a model of the compressor. There is thus no link, between the turbo model and the input of fresh air, in the intake manifold (see Figure 4.1). Still a model of the turbine is necessary in order to calculate W_{Turb}, needed in (4.10) for conservation of mass.

The mass-flow through the turbine is modeled as

$$W_{Turb} = \frac{p_{Exh}}{\sqrt{T_{Exh}}} g\left(\frac{p_{Exh}}{p_{Turb}}, l_{VNT}\right),\qquad(4.12)$$

where the look-up table g, provided by the manufacturer is shown in Figure 4.6. It has been normalized as:

$$g\left(\frac{p_{Exh}}{p_{Turb}}, l_{VNT}\right) = W_{Turb}\frac{\sqrt{T_{Exh}}}{p_{Exh}}.\qquad(4.13)$$
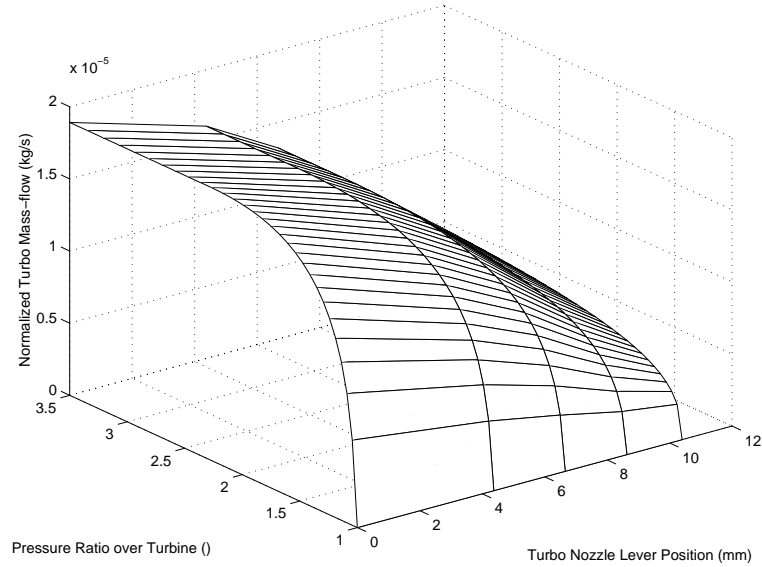

Figure 4.6: Look-up table g.

The look-up table $g\left(\frac{p_{Exh}}{p_{Turb}}, l_{VNT}\right)$ is a function of pressure ratio over the turbine and the position, in mm, of the nozzle lever. The pressure before the turbine is clearly the exhaust pressure, p_{Exh} (see Equation (4.11)), but it is necessary to look closer at the pressure after the turbine, p_{Turb}.

It will be attempted in the following two subsections to improve the existing turbine model. It was decided in an early stage of this project to stay with the original turbine model and try to improve it, rather than looking at alternative solutions.

4.4.1   Turbine Pressure Model

The pressure ratio over the turbine used as input to look-up table g, has in the previous work with this model been:

$$c_1 + c_2 \frac{p_{Exh}}{p_{Turb}} + c_3 \left(\frac{p_{Exh}}{p_{Turb}} \right)^2 , \qquad (4.14)$$

where c_{1-3} are constants, that have been calculated using a least-square fit to measurement data. However, it is shown in Section 6.3, that the results of this are not perfect. It is therefore necessary to look at alternative solutions.

Exhaust pressure is modeled using conservation of mass in the exhaust manifold. But how should the pressure after the turbine be modeled? It could be assumed that:

$$p_{Turb} = p_{Amb}. \qquad (4.15)$$

That means that there would be the same pressure, all the way through the exhaust pipe. That is not true for normal engine operation. This is shown in Figure 4.7 where both p_{Amb} and p_{Turb} are plotted. The pressure after the turbine, increases with increased fueling and engine speed, due to increased mass-flow, through the exhaust-pipe. It will here be investigated, if it is possible to make a model of the pressure, after the turbine, without adding another state equation. Adding a state, would increase the complexity of the model and thereby slow down simulations, an unwanted effect. Two different approaches will be described below and they will then be validated in Section 6.3, to see, how they affect the system.

The first approach is to create a static 2D look-up table describing pressure increase after the turbine, as a function of fueling and engine speed; $k(N_{Eng}, X_{Inj})$. This can be done, using the roll testbed data, described in Section 4.2. The table is shown in Figure 4.8 and would be implemented as:

$$P_{Turb} = P_{Amb} \cdot k(N_{Eng}, X_{Inj}). \qquad (4.16)$$

It can be seen in Section 6.3, that the results of the above described look-up table, indeed are satisfying. The aim of this thesis is to make a
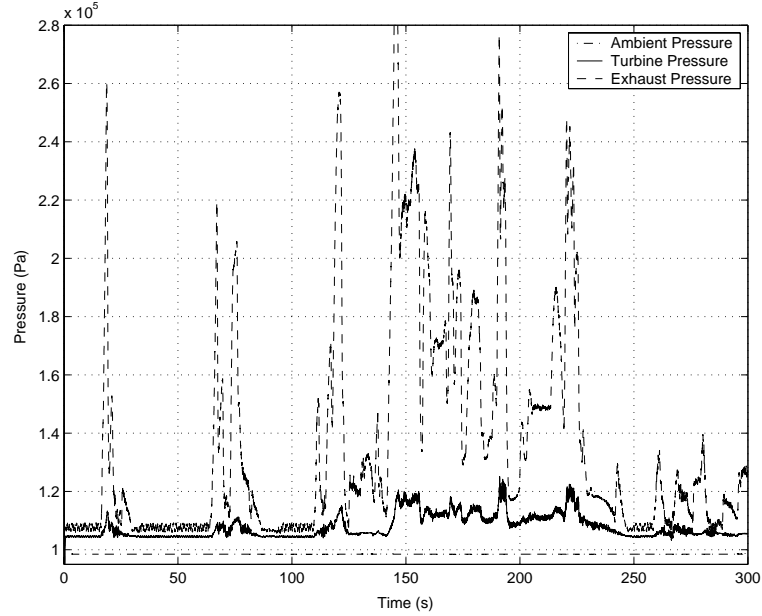
Figure 4.7: Measured ambient-, turbine- and exhaust pressure for mixed city- and highway driving conditions.

model for diagnosis purposes. Using this table would disable the possibility, to perform diagnosis of e.g. leakage in the exhaust manifold. This is because, the pressure after the turbine is modeled using signals, that are not in direct connection with the turbine. Pressure after the turbine, is thus made independent, from the local system. If a fault appeared, there would thereby be difficulties, in telling where, in between e.g. the fuel injector and the turbine, it was that the fault was caused.

This is a simple way to estimate p_{Turb}. But it disables the possibility, for fault diagnosis of the system. It would be necessary to make a model of the exhaust pipe to get around this problem. It could be modeled as a normal flow restriction. The pressure after the turbine, is thus built up when the mass-flow through the exhaust pipe is restricted. A normal restriction [11] for an incompressible, gas can be modeled as:

$$W_{Restriction}^2 k_1 T_{Turb} = p_{Turb}(p_{Turb} - p_{Amb}). \qquad (4.17)$$

where k_1 is a constant and $W_{Restriction}$ is the mass-flow going into the restriction and then out to the atmosphere, that has ambient pressure. It can be assumed that the gas is incompressible, since the pressure difference, over the restriction, is relatively small (see Figure 4.7). For this system, $W_{Restriction} = W_{Turb}$ in (4.17). However, p_{Turb} would then
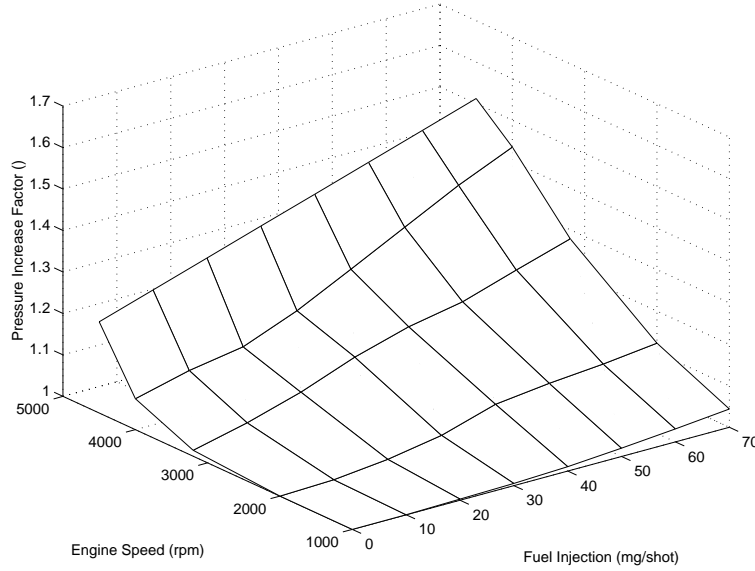
Figure 4.8: Pressure increase after turbine look-up table.

be a function of W_{Turb}, and according to (4.12), W_{Turb} is a function of p_{Turb}. It is thus necessary to include a reservoir, after the intake turbine (see Figure 4.9), to make the equations solvable for Matlab. Including the reservoir, means that a new state, built on the conservation of mass equation, will have to be added to the model. This would be:

$$\dot{m}_{Reservoir} = W_{Turb} - W_{Restriction}, \tag{4.18}$$

where $\dot{m}_{Reservoir}$ is the change in mass of gas, in the reservoir. However, simulation time is severely increased by increasing the number of states in the model and that is, as already mentioned, an unwanted effect.
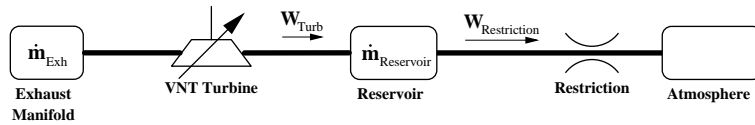

Figure 4.9: Schematic overview of how a reservoir would be included in the model.

The second approach to model the pressure after the turbine is based on the fact that p_{Turb} is used only to calculate the pressure ratio over the turbine as an input to look-up table g (see Equation (4.12)). A

closer look at look-up table g in Figure 4.6 shows that if a small change in $\frac{p_{Exh}}{p_{Turb}}$ is applied, a large change in turbine mass-flow is obtained when the pressure ratio is small. When the pressure ratio is large, on the other hand, is a smaller change in mass-flow obtained for a small change in $\frac{p_{Exh}}{p_{Turb}}$. This means, that the mass-flow model is more sensitive to an error in p_{Turb} or p_{Exh}, for low- than for high pressure ratios. Low pressure ratios over the turbine, typically occur for low power output of the engine, e.g. for idling speed. An example of the relationship between exhaust pressure and pressure after the turbine is shown in Figure 4.7. It is here intended to construct a model for p_{Turb}, that is correct for idling speed, since this seem to be the operating point, where the influence of error in p_{Turb} is the largest.

An implementation of the reservoir would show, that the values of $\dot{m}_{Reservoir}$ are so small, that it is neglectable, compared to W_{Turb} in (4.18). The assumption that $W_{Restriction} = W_{Turb}$ can thus be made. It is also assumed, that both the mass-flow through the turbine and the exhaust temperature are constant at idling speed. The assumptions made, make everything on the left side, of the equal sign, in (4.17) constant. This constant can be identified from measurements made during idling speed:

$$k = mean\{p_{Turb}(p_{Turb} - p_{Amb})\} = 5.75 \cdot 10^8. \qquad (4.19)$$

By using (4.17), p_{Turb} can be expressed as:

$$p_{Turb} = \frac{p_{Amb} + \sqrt{p_{Amb}^2 + 4k}}{2} \qquad (4.20)$$

This is hence a model that does not disable any faults for the diagnostics system. It is ,on the other hand, dependent on constant exhaust mass-flow and temperature at idling speed. This may not be completely correct, if the entire life cycle of an engine is considered.

The simulation results of the two approaches, along with the results of the original model and the model using only p_{Amb}, will be presented in Section 6.3.

4.4.2 VNT Actuator Model

The second input to the table g, in (4.12), is the position in mm of the nozzle lever. The nozzle lever is the mechanical link between the VNT actuator and the vanes. The position of the lever is very difficult to measure. However, the VNT actuator control signal, X_{VNT} (in %), can easily be measured from the ECU. In the previous work with this model, it was assumed, that nozzle lever position is a linear function of the actuator control signal:

$$l_{VNT} = X_{VNT} \frac{10.4}{100}, \qquad (4.21)$$

where 10.4 mm is the movable length of the nozzle lever.

It will be attempted to create a more precise model of the lever position. This can be done by creating a table that transforms X_{VNT} into l_{VNT}. The nozzle lever position has to be estimated from some other measurable variable, since there is no sensor for l_{VNT}. Estimated nozzle lever position, $\hat{l}_{VNT}$, can then be calculated by using the model equations. The transformation table is then created by fitting a polynomial between $\hat{l}_{VNT}$ and X_{VNT}. It would be optimal to estimate $\hat{l}_{VNT}$ from the turbine mass-flow, W_{Turb}, but it is not measureable, without changing the characteristics of the system. The closest measurable signals are pressure and temperature, in the exhaust manifold and they will thus be used to estimate $\hat{l}_{VNT}$. Equations (4.10) and (4.11) give:

$$W_{Turb} = W_{Exh} - \frac{\delta}{\delta t}\left(\frac{p_{Exh}V_{Exh}}{R_{Exh}T_{Exh}}\right) \qquad (4.22)$$

if EGR is turned off. A derivation has to be made to calculate W_{Turb}. This had to be approximated using a numerical differentiation filter [12], since noise in the measured signals, caused a normal derivation to give inaccurate results. The differentiation filter is

$$\bar{\dot{m}}_{Exh} = \frac{s}{\tau s + 1}\left(\frac{p_{Exh}V_{Exh}}{R_{Exh}T_{Exh}}\right), \qquad (4.23)$$

with a time constant τ, chosen as small as possible without excessively amplifying noise. Having done this, it is possible to calculate $\bar{\dot{m}}_{Exh}$. The result shows that the value of $\bar{\dot{m}}_{Exh}$ is so small, that it is neglectable, compared to W_{Exh} in (4.22). It can thus be assumed that:

$$W_{Turb} = W_{Exh}. \qquad (4.24)$$

Then (4.12) gives:

$$\hat{l}_{VNT} = f\left(\frac{W_{Exh}\sqrt{T_{Exh}}}{p_{Exh}}, \frac{p_{Exh}}{p_{Turb}}\right) \qquad (4.25)$$

where f is table g, inverted to produce l_{VNT}, as a function of the output of g and $\frac{p_{Exh}}{p_{Turb}}$. Inverting the table caused some minor numerical difficulties, because Simulink only accepts a square output matrix for 2D look-up tables. This could however be solved by extrapolating the original table prior to inverting it. Table f is shown in Figure 4.10. Figure 4.6 shows that table g is invertible for all points, except for when

$\frac{p_{Exh}}{p_{Turb}} \to 1$. For this point there exist several l_{VNT} outputs from table f, but in practice only one is used. This particular output is however unknown, so the fit has to be limited only to be made on measurement data, that do not include points where $\frac{p_{Exh}}{p_{Turb}} \to 1$. A set of data can now be generated from measured data with (4.25), to fit a polynomial to. The fit is a least-square fit and it is shown in Figure 4.11.
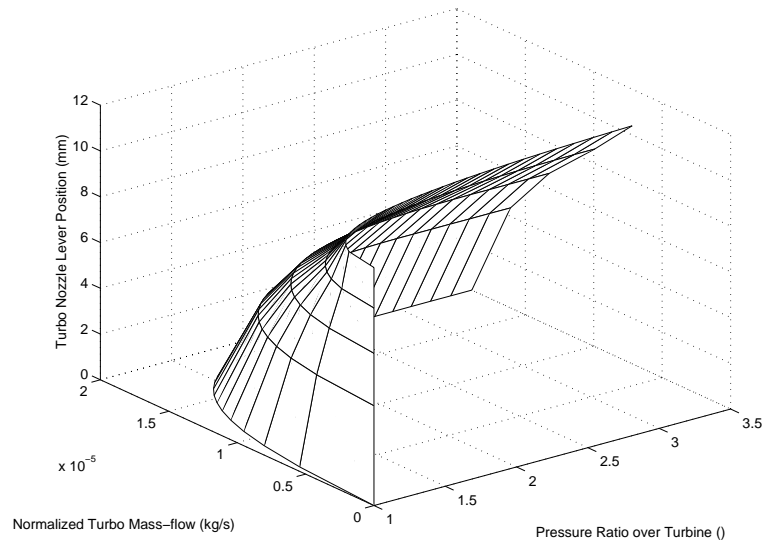

Figure 4.10: Look-up table f.

The VNT control signal, X_{VNT}, is defined between 5% (vanes fully open) and 95% (vanes fully closed). The fit in Figure 4.11 starts first at 40% X_{VNT}. The reason for this is that the range of VNT control signal below 40% seems to be used, only during hard accelerating driving conditions. It seems to be represented only by transients. As so, it would be impossible to make a measurement valid for steady state equations. If the fit was made to transient data, a map would be obtained, that compensates for, that the exhaust model is unable to model transients accurately. Therefore, the table transforming X_{VNT} into l_{VNT} is defined only from 40%. Simulink will extrapolate for values below 40% during simulations. This is acceptable, since the range of control signals below 40% always are very short term and their influence on a mean value model, can therefore be neglected. Control signals in the range 85% to 95% does not seem to be used very often. Simulink will extrapolate also in this region.

The main problem of the fit is, that any model errors in the exhaust- and turbine models will be included in the fit. This is especially im-
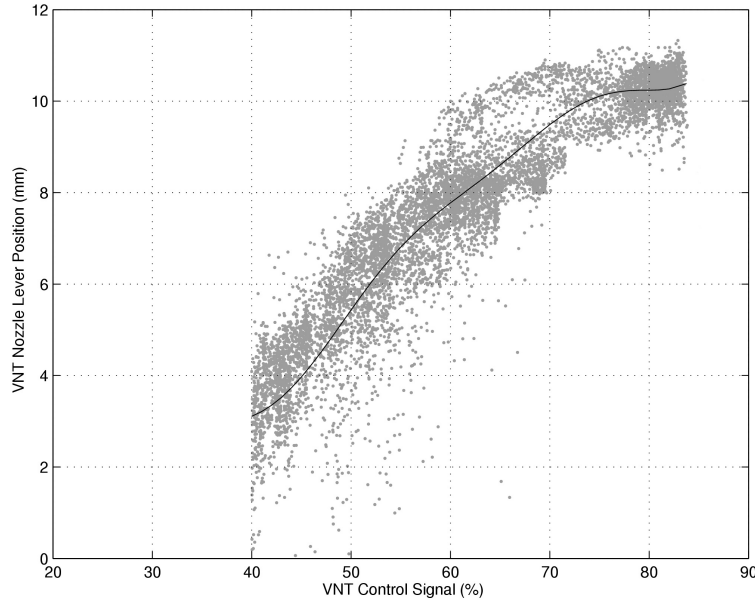
Figure 4.11: Least-square polynomial fit of $\hat{l}_{VNT}$ to X_{VNT}, plotted over data fitted to.

portant, since the purpose of the model is, that it should be the basis for a model based diagnostics system. Such a system should be able to identify faults, in different parts of the engine. The model should therefore not compensate for errors, in e.g. the exhaust manifold model, in the model of the turbine. One part of the measurement data used for the fit, can be shown to be caused by faults, in some other part of the model. An example of this fault, taken from a different part of the same measurement file, is shown in Figure 4.12. The data shown there does not fit well with the other data shown in Figure 4.11. It was initially believed, that the look of the data was caused by a hysteresis in the VNT actuator. However, trials with hysteresis included in the actuator model showed, that so was not the case. The actual reason for this seems to be, that the data was sampled during a quick response in VNT area change, this caused a transient, since neither the exhaust or the turbine model manages quick responses very well. The aim was to exclude data, where this occurs, from the data used as basis for the X_{VNT}, l_{VNT} fit. That was not possible, since it is necessary to have a large set of data, to make the fit from and the transients occur quite frequently, e.g. with gear shifting. Similar data to those shown in Figure 4.12, are therefore also present in the data, used for

the fit (Figure 4.11). This has probably affected the fit, but there is no way of avoiding this. The data shown in Figure 4.12 includes points where $\frac{p_{Exh}}{p_{Turb}} \rightarrow 1$. This is obvious at 85% VNT control signal, which corresponds to idling speed.

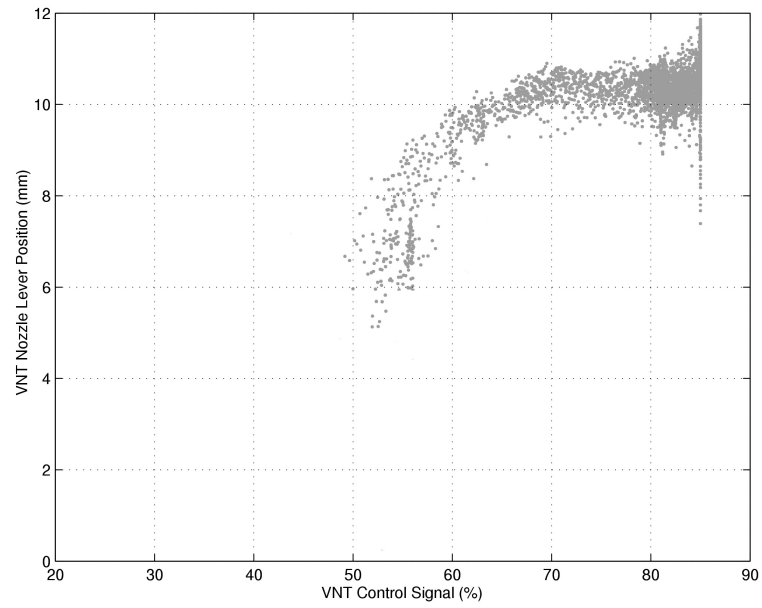The table transforming X_{VNT} into l_{VNT} will be validated in Section 6.3.

Figure 4.12: Example of data that should not be included in the X_{VNT}, $\hat{l}_{VNT}$ fit.

Chapter 5

EGR Model

This chapter takes a closer look at the modeling of the EGR system. Steps were taken, in Chapter 4, to get a good model of the engine with EGR turned off. With that as basis, the model will here be extended with the EGR system. The EGR model is built on the same basis as the engine model.

The EGR system takes EGR gases from the exhaust manifold, through a special pipe and then injects them in the normal air flow, just before the intake manifold. The amount of gases recirculated are governed by a valve. The layout of the EGR system is shown in Figure 5.1.
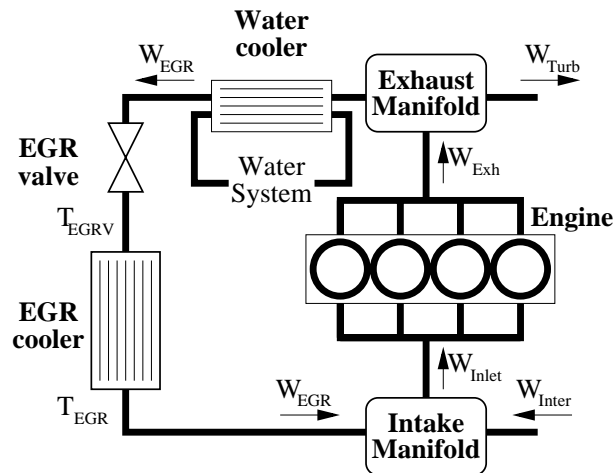

Figure 5.1: Schematic overview of the EGR system.

5.1   Mass-flow Model

One of the conclusions in [1] and [2] is, that the EGR system of this model, seem to give very bad results during simulations. This was believed to be caused by a hysteresis effect in the EGR valve actuator. It was therefore decided, in the initial state of this project, that a new EGR valve, without this hysteresis effect, should be installed. The previous valve was a pneumatically controlled valve and it was believed, that it was during compression of the air in the pneumatic actuator, that the hysteresis occurred. The EGR valve was therefore replaced. The new valve installed is electrically controlled so that less hysteresis should occur.

It is shown in Figure 5.1, that a water-cooler is connected to the exhaust manifold. The EGR valve is positioned after this followed by the EGR-cooler. This setup is for the new electrically controlled valve. The old valve was positioned after the EGR-cooler. The first thing to be done was to rearrange the existing EGR model in order to correspond to the new setup. That model will be presented here. It is assumed that there is no pressure drop over the water-cooler and the EGR-cooler.

The mass-flow through the EGR valve needs to be modeled. The model used previously can be found in [5]. It assumes an ideal gas with constant specific heats. It is thus a model for a compressible gas and its basis is the steady flow energy equation. The resulting model is governed by a condition called *choked or critical flow*. This means that the maximum mass-flow, through the valve occurs, when the velocity at the minimum area of the valve (the throat) equals the velocity of sound. The following relation for choked flow:

$$\frac{p_{Intake}}{p_{Exh}} \quad = \quad \left(\frac{2}{\gamma_{Exh}+1}\right)^{\frac{\gamma_{Exh}}{\gamma_{Exh}-1}},$$

is called the critical pressure ratio. It is 0.53 for γ_{Exh}.

The EGR valve mass-flow model summarized:

$$W_{EGR} \quad = \quad \frac{p_{Exh}A_{EGRV}}{\sqrt{R_{Exh}T_{Exh}}}\Psi_{\gamma_{Exh}}\left(\frac{p_{Intake}}{p_{Exh}}\right), \qquad (5.1)$$

where

$$\Psi_\gamma\left(\frac{p_1}{p_0}\right) = \begin{cases} \sqrt{\frac{2\gamma}{\gamma-1}\left[\left(\frac{p_1}{p_0}\right)^{\frac{2}{\gamma}} - \left(\frac{p_1}{p_0}\right)^{\frac{\gamma+1}{\gamma}}\right]} \\ \qquad\qquad \text{if } \left(\frac{p_1}{p_0}\right) \geq \left(\frac{2}{\gamma+1}\right)^{\frac{\gamma}{\gamma-1}} \\ \\ \sqrt{\gamma\left(\frac{2}{\gamma+1}\right)^{\frac{\gamma+1}{\gamma-1}}} \qquad \text{otherwise} \end{cases}$$

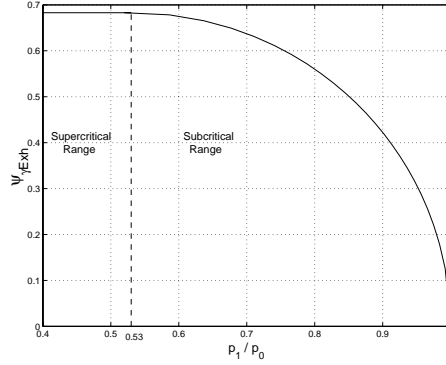The function $\Psi_{\gamma_{Exh}}$ has been implemented in Simulink as a table. The table is shown in Figure 5.2.

Figure 5.2: The flow function $\Psi_{\gamma_{Exh}}(p_1/p_0)$ with supercritical and sub-critical range shown.

The parameter A_{EGRV} is the effective area of the new EGR valve. This is then the real area multiplied by a discharge coefficient, C_D:

$$A_{EGRV} = C_D A_{Real}.$$

The effective valve area, A_{EGRV}, was supplied by the valve manufacturer. Different effective area curves, for different pressure ratios over the valve were given. The difference for different pressure ratios was so small, that it was neglectable. Simulations with the effective area, provided by manufacturer gave bad results. It was therefore decided, that an effective area should be estimated from the measurement system, installed in the research car. It would be optimal to make a least-square fit to the EGR mass-flow, W_{EGR}, but this is not measureable without disturbing the characteristics of the system. The closest measurable signals, useful for validation are in the intake manifold. The EGR mass-flow can be calculated from (4.3):

$$W_{EGR} \quad = \quad \frac{1}{T_{EGR}} \cdot \left[\frac{\dot{p}_{Intake} V_{Intake}}{\gamma_{Intake} R_{Intake}} + W_{Inlet} T_{Intake} - \quad (5.2) \right.$$
$$\left. -W_{Inter} T_{Inter} + \frac{\dot{q}_{Intake}}{c_{p,Intake}} \right],$$

where

$$\dot{q}_{Intake} = h_{HT}(T_{Intake} - T_{Wall}).$$

A derivation of the measured intake manifold pressure is necessary. This had to be approximated using a numerical differentiation filter [12], because noise in the measured signal caused a normal derivation to give inaccurate results. The differentiation filter is

$$\bar{\dot{p}}_{Intake} = \frac{s}{\tau s + 1} p_{Intake},$$

with a time constant τ chosen as small as possible, without excessively amplifying noise. It is also necessary to do the corresponding filtering:

$$\bar{W}_{Inlet} = \frac{1}{\tau s + 1} W_{Inlet}, \quad \bar{W}_{Inter} = \frac{1}{\tau s + 1} W_{Inter},$$

$$\bar{\dot{q}}_{Intake} = \frac{1}{\tau s + 1} \dot{q}_{Intake},$$

to get

$$\hat{W}_{EGR} = \frac{1}{T_{EGR}} \cdot \left[\frac{\bar{\dot{p}}_{Intake} V_{Intake}}{\gamma_{Intake} R_{Intake}} + \bar{W}_{Inlet} T_{Intake} - \right. \tag{5.3}$$
$$\left. - \bar{W}_{Inter} T_{Inter} + \frac{\bar{\dot{q}}_{Intake}}{c_{p,Intake}} \right].$$

There is no need to filter the temperatures since their dynamics are so slow. It is then possible to calculate $\hat{A}_{EGRV}$ from (5.1) as:

$$\hat{A}_{EGRV} = \frac{\sqrt{R_{Exh} T_{Exh}}}{p_{Exh} \Psi_{\gamma_{Exh}} \left(\frac{p_{Intake}}{p_{Exh}} \right)} \hat{W}_{EGR}.$$

This is possible only if $\Psi_{\gamma} \left(\frac{p_1}{p_0} \right)$ is invertible. Figure 5.2 shows that it is.

A set of data can now be generated from $\hat{A}_{EGRV}$ and the EGR valve control signal, X_{EGRV}, to fit a polynomial to. The fit is a least-square fit and it is shown in Figure 5.3. The results of the entire EGR valve model will be shown in Section 6.4.1.

An extensive literature search was made on EGR models. It seems that the model presented in this thesis, is the most detailed MVEM model of EGR systems, that is used [5,12,13]. Some literature suggests a model assuming that the EGR gases are incompressible [14]. However, an incompressible assumption is less realistic than assuming ideal gas so this was not chosen to be implemented.

Another issue to look into would have been how pulsations in the EGR gas affects the MVEM model. The EGR valve model would estimate that there is no mass-flow, when the mean pressure ratio over the valve is close to unity. If there in reality is a pulsation, then there
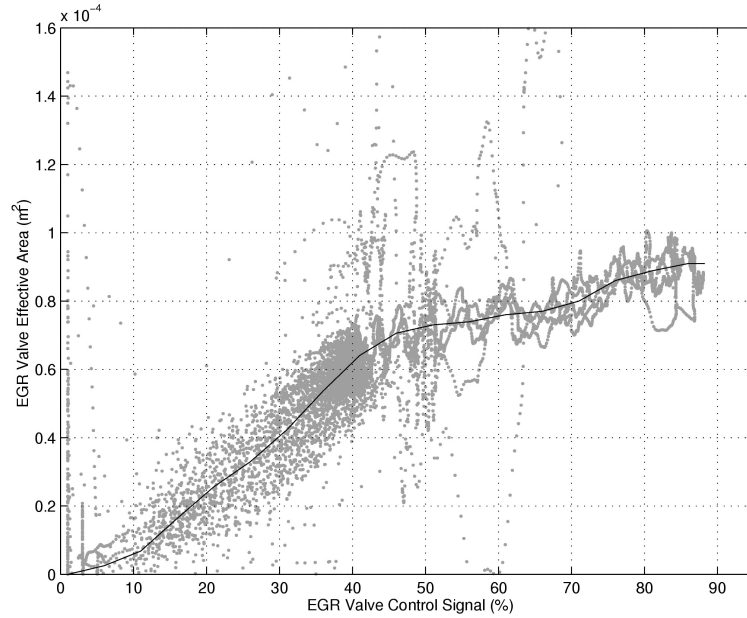
Figure 5.3: Polynomial least-square fit of X_{EGRV} to $\hat{A}_{EGRV}$, plotted over the data that was basis for the fit.

would be a small mass-flow, even if the mean pressure ratio is unity. This would thus cause an error. It is shown in Section 6.4.1 that the EGR model works very well. This could mean either that the influence of pulsations are very small, or that a compensation for pulsations has been included in the identification of the A_{EGRV} map. However, since the results are good, the pulsation issue were neglected and more effort were instead put into modeling of the inputs to the EGR model: p_{Intake} and p_{Exh}. T_{Exh} is considered to already be modeled well enough. Modeling of p_{Intake} and p_{Exh} has already been shown in Chapter 4.

5.2 Temperature Model

The main purpose of the water-cooler is actually not only to cool the EGR gases. It is also used to heat up the cooling water for cold driving conditions. It is therefore assumed, that the water-cooler affects the EGR gas only when the engine is cold. The diagnostics system that this model is purposed for, is not intended to work for a cold engine and hence the water-cooler can be neglected. It is assumed that there

is no temperature drop over the EGR valve, i.e.:

$$T_{EGRV} = T_{Exh}. \tag{5.4}$$

The EGR-cooler is modeled as a normal heat-exchanger. The temperature after the EGR cooler can be calculated by neglecting the pressure drop over the cooler:

$$T_{EGR} = T_{EGRV} + k \cdot \epsilon_{EGRC} \cdot \Delta T. \tag{5.5}$$

where ϵ_{EGRC} is the effectiveness of the cooler. This has been calculated from static engine testbed data and is implemented as a function of mass-flow through it and engine speed. It is shown in Figure 5.4. Measurements showed that it was necessary to complement ϵ_{EGRC} with a factor k. The constant probably makes up for heat losses in the water-cooler and the normal pipes. It could also be a compensation for the changes from making measurements in a static testbed to using the cooler in a real car. The variable ΔT represents the temperature difference between the gases in the cooler, T_{EGRV}, and the outside of the cooler, i.e. the temperature under the hood. The latter has already been modeled in Section 4.1.1 as T_{Wall}. This gives:

$$\Delta T = T_{EGRV} - T_{Wall}. \tag{5.6}$$

In the original model, ΔT was modeled as $T_{EGRV} - T_{Water}$ where T_{Water} is the temperature of the engine cooling water. T_{Water} was used since T_{Wall} had not yet been modeled.

It has been argued in [3], that the influence of EGR temperature is so small that it is sufficient to keep it constant. The original model has been used with constant EGR temperature. Therefore also this approach will be evaluated. The temperature has been set to $831K$.

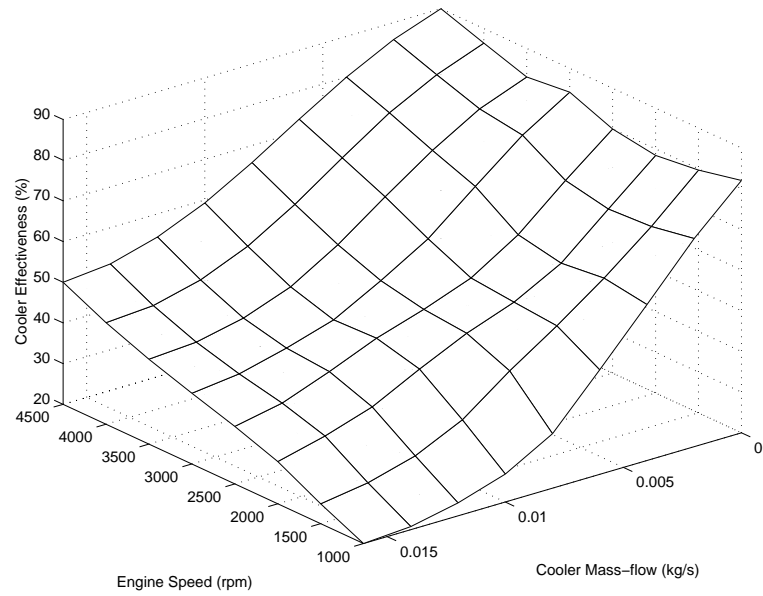The results of the EGR cooler model will be shown in Section 6.4.2.

Figure 5.4: EGR-cooler effectiveness look-up table

Chapter 6

Validation

This chapter describes validation and comparison of the different submodels presented in Chapter 4 and 5. The submodels will be validated in the order they have been presented there. When all submodels have been validated, a resulting model can be put together from the different submodels that proved to be the best. This resulting model, will in the last section, be validated and compared with the original model.

To make the validations, simulated quantities will be compared with measured quantities. It is important not to use the same measurement data for validation as for identification. It is necessary to make measurements for different driving conditions in order to make a proper validation. It is also necessary to make measurements during a relatively long time so that not only one special operating point is captured. All validation measurement files are therefore 5 minutes long. All measurements are made with a hot engine. No measurements have been made during cold start or warming up. The different kinds of driving conditions, used for validation, are:

- **Mixed driving:** Half the measurement is made during city driving with several idling speed stops at traffic lights and the other half is made on a medium highway.

- **Highway driving:** Measurement made during fast highway driving.

- **Uphill driving:** Measurement made during low speed uphill driving so that high load conditions can be validated. Includes idling speed stops at traffic lights.

The engine speed and fueling profile for each validation measurement are presented in Appendix A. The measurements have been made, driving the same cycle, both with and without EGR so that the influence of EGR on the model can be validated. EGR measurements have

41

been made both with the old and the new EGR valve. The EGR valve
is normally controlled by the ECU. This means that the valve opens
and closes to control the flow of EGR gases, recirculated into the intake
manifold (see Section 2.2). EGR is turned off by overriding EGR con-
trol signal so that it constantly gives a value of 3%, which corresponds
to a closed valve. In the first sections (Sections 6.1 to 6.3) below, the
engine model without EGR will be validated and then in the EGR
section (Section 6.4), the EGR system will be validated. The entire
model, both with and without EGR, will be validated in the final sec-
tion. There will also be a comparison between the new model with the
new EGR valve with the original model with the old EGR valve.

It is necessary to define a measure for what errors the models causes,
in order to validate. The reference will always be measured quantities.
The measures that will be used are mean error, RMS error and maxi-
mum error:

$$e_{mean} = \frac{1}{n}\sum_{i=1}^{n}\frac{|\hat{x}(t_i) - x(t_i)|}{x(t_i)}, \tag{6.1}$$

$$e_{RMS} = \frac{1}{n}\sum_{i=1}^{n}\frac{\sqrt{(\hat{x}(t_i) - x(t_i))^2}}{x(t_i)}, \tag{6.2}$$

$$e_{max} = \max_{1\leqslant i\leqslant n}\frac{|\hat{x}(t_i) - x(t_i)|}{x(t_i)}. \tag{6.3}$$

where n is the number of samples, $\hat{x}$ is a simulated quantity and x is a
measured quantity.

6.1   Intake Manifold Model Validation

The two different intake manifold models that have been presented in
Section 4.1 will be validated in this section. The idea is to compare
them so that the best possible intake manifold model is used to base
other modeling on. The validation has therefore been done using mea-
surement files where EGR is turned off.

The pumping model will affect the results of the intake manifold
model as can be seen in Figure 4.1. The reason is that W_{Inlet} is in-
cluded in the intake manifold equations. The generation of volumetric
efficiency maps is independent of which intake manifold model is used,
as seen in (4.7). The volumetric efficiency map that gives the best re-
sults in Section 6.2 can therefore be used here. Measurements with the
model that includes heat transfer has been made using the model for
T_{Wall} that is presented in Section 4.1.1 instead of the measured T_{Wall}.
The reason for this is that it is necessary to evaluate the practical capa-

bilities of the model, since the sensor for T_{Wall} only has been installed temporarily for modeling purposes.

   To validate the intake manifold models there are in practice only pressure and temperature that are measurable. Therefore, p_{Intake} and T_{Intake} will be used as quantities when the different errors in equations (6.1) to (6.3) are calculated. This will be done for the three different types of driving conditions and the results are presented in Table 6.1.

Model-states	Pressure Errors (%)			Temperature Errors (%)		
	e_{mean}	e_{RMS}	e_{max}	e_{mean}	e_{RMS}	e_{max}
Mixed driving						
$p\&m$	1.93	2.25	5.62	8.87	10.44	33.91
$p\&T+HT$	1.52	2.13	12.32	7.19	9.17	22.75
Highway driving						
$p\&m$	2.81	3.37	8.98	6.42	8.11	35.18
$p\&T+HT$	1.75	2.31	8.76	1.95	2.42	7.86
Uphill driving						
$p\&m$	1.57	1.83	6.36	10.39	11.62	35.18
$p\&T+HT$	1.45	2.08	14.43	8.20	9.62	25.13

Table 6.1: Intake manifold pressure- and temperature errors for different models and driving conditions.

   RMS errors are always larger than mean errors. This is because of the squaring of the errors. This means that larger errors will be weighted more than small errors and thus the influence of peaks is larger on RMS error than on mean error.

   The pressure and temperature state model with heat transfer is superior in modeling temperature for all three types of errors. But temperature cannot be considered to be as important as pressure. The only fault in the diagnostics system that is directly dependent on intake manifold temperature is fault in the T_{Inter} sensor. Pressure on the other hand is used to detect faults in e.g. intake manifold leakage, error in W_{Inter} sensor or stuck EGR valve. But temperature affects the pressure state. Partly since T_{Intake} is included in the pressure state equation, but also since intake temperature is used to calculate the density (see (4.9)), used as input to the volumetric efficiency map (4.7). The latter proved to be very sensitive. The pressure and temperature state model with heat transfer is superior also in mean error of pressure simulation. And in two out of three cases also for RMS errors. The main advantage of the pressure and mass state model is that it seems to have very low maximum errors. This is what causes the better RMS error for the uphill driving condition.

The pressure and temperature model with heat transfer were chosen as basis for the continued work in this thesis. The reason is that it has superior mean pressure error and better temperature modeling. This model does have a higher maximum error, but peaks in the error can be filtered as long as they do not contain too much energy. The RMS error weights peaks more than the mean error and even then this model is better in pressure simulation in two out of three cases. The energy in the peaks can thus not be too great.

6.1.1   Wall Temperature Model Validation

To validate the model of the intake manifold temperature, errors against measured T_{Wall} will be considered. This is presented in Table 6.2 and an example is plotted in Figure 6.1.

	Temperature Errors (%)		
	e_{mean}	e_{RMS}	e_{max}
Mixed driving	6.47	7.62	18.18
Highway driving	16.35	16.49	23.79
Uphill driving	11.16	11.62	19.43

Table 6.2: Errors in the model of temperature on the intake manifold wall.
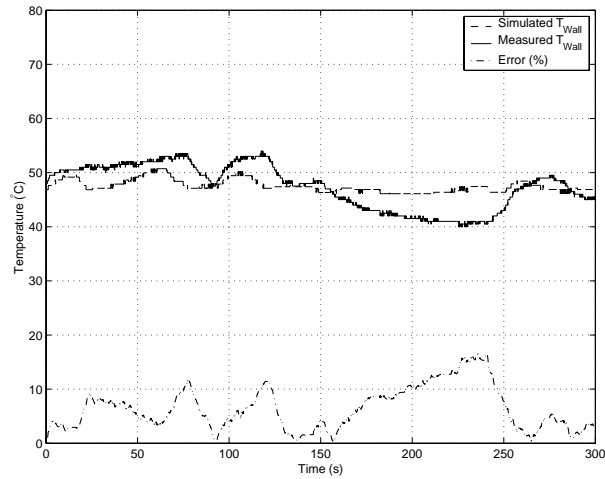

Figure 6.1: An example of how the model of T_{Wall} behaves compared to measured values; Mixed driving.

The model works fairly well even though it is very simple. It can of course not capture all the dynamics of the temperature but the error rarely exceeds $10°C$. The model gives different offsets to the measured values for different measurement files. Even if they are for the same outdoor conditions. This could be explained by the fact that the fan is not included in the model (see Section 4.1.1) and that no heat transfer through the hood is considered. This would explain why there are better results for mixed driving, since the model fit was made for a measurement file with mixed driving.

It is also necessary to consider what influence the errors caused by the T_{Wall} model have on the intake manifold model. Table 6.3 presents errors in the heat transfer model both for modeled and measured T_{Wall}. The volumetric efficiency map that was concluded to be the best, in Section 6.2 was used.

T_{Wall}	Pressure Errors (%)			Temperature Errors (%)		
	e_{mean}	e_{RMS}	e_{max}	e_{mean}	e_{RMS}	e_{max}
Mixed driving						
Measured	1.48	2.11	13.56	9.57	11.64	24.64
Simulated	1.52	2.13	12.32	7.19	9.17	22.75
Highway driving						
Measured	1.73	2.29	9.09	4.91	5.36	10.75
Simulated	1.75	2.31	8.76	1.95	2.42	7.86
Uphill driving						
Measured	1.27	1.91	13.16	16.14	17.10	27.05
Simulated	1.45	2.08	14.43	8.20	9.62	25.13

Table 6.3: Intake manifold pressure- and temperature errors for the heat transfer model both with measured and simulated T_{Wall}.

It is clear that even though there is up to 24% error in the intake manifold wall temperature, the effect thereof on intake manifold pressure is not great. It seems that the magnitude of the errors in Table 6.2 do not correspond to the mean pressure errors in Table 6.3. This must mean that for these three results, the errors in the T_{Wall} model compensates for errors in the intake manifold model. This also seems to be the case for the temperature model, where the errors are smaller for modeled T_{Wall} than for measured T_{Wall}. It has not been investigated further how the temperature model results can be better than the results for measured temperature. It has to be considered that the errors just as well could be far worse than the three cases presented in Table 6.3, when the error in T_{Wall} doesn't compensate, but works in the other direction on the intake manifold model.

6.2   Pumping Model Validation

There is no direct way to validate the different volumetric efficiency maps generated in Section 4.2. To validate volumetric efficiency it would be needed to measure the actual flow of air going into the cylinders. Since there is no sensor for this, there is no way to make a validation with simulated and measured W_{Inlet}. The closest measurable signals in the model are intake manifold temperature and pressure. They are both directly affected by W_{Inlet}. Hence a comparison of the volumetric efficiency maps can be made by looking at intake manifold pressure and temperature. However, this does not generate a measure of how good a certain volumetric efficiency map is. A comparison can only be made to tell which map best fits the intake manifold model. There is no way of telling which map it is that best predicts the flow of air into the cylinders in a correct way.

The results in Section 6.1 were dependent on the results in this section and the results in this section are dependent on the results there. To solve this it was necessary to evaluate all combinations of intake manifold models and volumetric efficiency maps. Since it was concluded in Section 6.1 that the pressure and temperature state model with heat transfer is the superior intake manifold model, only the results for this model will be presented here. The basis for the comparison is again measurement files with EGR turned off. Measured T_{Wall} will be used, so that focus is put only on the difference caused by the volumetric efficiency maps.

First the two different maps in Section 4.2.1 will be compared to see if there is any back-flow from the cylinder, affecting the temperature sensor in the intake manifold. The results are presented in Table 6.4 where the map generated with T_{Intake} is called map 1 and the map generated using T_{Inter} is called map 2. The results in Table 6.4 show that the differences in both pressure and temperature errors are small, if T_{Inter} is used instead of T_{Intake} in the generation of the volumetric efficiency map. Hence the effect of back-flow from the cylinders on the temperature sensor in the intake manifold, can almost be taken as neglectable. The map generated with T_{Intake} is slightly better so this is the map that will be used as basis for the complement with new measurement points in Section 4.2.2.

Secondly the volumetric efficiency map that has been complemented with extra measurement points (see Section 4.2.2) will be validated. This map is called map 3. Table 6.4 shows that the new (complemented) map is superior to the old (original). The new map was complemented mainly in the low engine speed area. In the measurement files used for validation there are low engine speeds both in mixed- and uphill driving, for traffic light stops. Table 6.4 shows that it is for these two driving conditions that the largest improvements are made by us-

Volumetric efficiency	Pressure Errors (%)			Temperature Errors (%)		
	e_{mean}	e_{RMS}	e_{max}	e_{mean}	e_{RMS}	e_{max}
Mixed driving						
map 1	5.33	7.60	15.83	7.20	9.19	22.44
map 2	5.47	7.68	16.03	7.20	9.19	22.55
map 3	1.48	2.11	13.56	9.57	11.64	24.64
Highway driving						
map 1	1.91	2.47	8.96	1.94	2.45	7.71
map 2	1.82	2.37	8.54	1.94	2.41	7.80
map 3	1.73	2.29	9.09	4.91	5.36	10.75
Uphill driving						
map 1	7.38	9.52	17.96	8.19	9.63	23.80
map 2	7.50	9.57	17.88	8.19	9.62	24.37
map 3	1.27	1.91	13.16	16.14	17.10	27.05

Table 6.4: Comparison of intake manifold pressure and temperature errors for different volumetric efficiency maps.

ing the new map. In the highway driving there is also an improvement, but not as big as in the other conditions, since hardly any low engine speed driving is made in this measurement. Temperature in the intake manifold is hardly at all affected by a change of volumetric efficiency.

In the future work this new volumetric efficiency map, map 3, will be used. It has been generated using T_{Intake} and then complemented with additional measurement points in the low engine speed area.

6.3 Turbo Model Validation

Just as in the pumping model, there is also for the turbine model no direct way to make a validation. Once again it would be optimal to validate against mass-flow and that is something that cannot be measured because of the high temperature of the exhaust gases. This time the closest measurable signals are in the exhaust manifold. It is possible to measure pressure in the exhaust manifold. The temperature is not interesting since it is assumed in the model that the temperature in the exhaust manifold equals the temperature of the exhaust gases coming out of the cylinders. Validating against the pressure in the exhaust manifold means, that it can only be identified how well the turbine model fits our exhaust manifold model. A validation of how accurate the mass-flow through the turbine is compared with the actual mass-flow can not be done. The validation is made with measurement data where EGR is turned off.

6.3.1   VNT Actuator Model Validation

Validation of the model of the VNT actuator model (see Section 4.4.2) is described here. The model is run with the same three validation files with EGR turned off as in the previous sections. This has been done with measured values of p_{Turb} inserted in the model so that it can be seen what errors it is that actually come from the VNT actuator model. The results of the original model, where the nozzle lever position was assumed to be a linear function of VNT control signal (see equation (4.21)), are compared with the results of the new model that was identified in Section 4.4.2. The results are shown in Table 6.5 and an example is plotted in Figure 6.2.

VNT lever model	Pressure Errors (%)		
	e_{mean}	e_{RMS}	e_{max}
Mixed driving			
Original model	4.53	7.06	40.29
New model	3.86	5.16	25.08
Highway driving			
Original model	3.87	5.09	30.82
New model	3.07	3.95	20.45
Uphill driving			
Original model	4.84	7.65	37.08
New model	4.08	5.34	23.09

Table 6.5: Comparison of errors in exhaust manifold pressure for two different VNT actuator models.

The new VNT actuator model built on the fit to measurement data is superior to the linear model for all three simulations. This model was chosen to be used in the coming work. A closer look in Figure 6.2 shows that the model has a steady state error of about 3-4% at low exhaust pressures, i.e. idling speed. This is something that ought to be avoidable but it is obviously not captured in the VNT actuator model. The highway driving validation measurement does not have much idling speed and Table 6.5 shows that the error are lower for that measurement.

6.3.2   Turbine Pressure Model Validation

When the size of the errors caused by the VNT actuator model are known, it can be validated how the different models of the pressure after the turbine will affect exhaust manifold pressure. Four different models have been covered in Section 4.4.1. The first one is the original model used. This was the one where a least-square fit was made to the
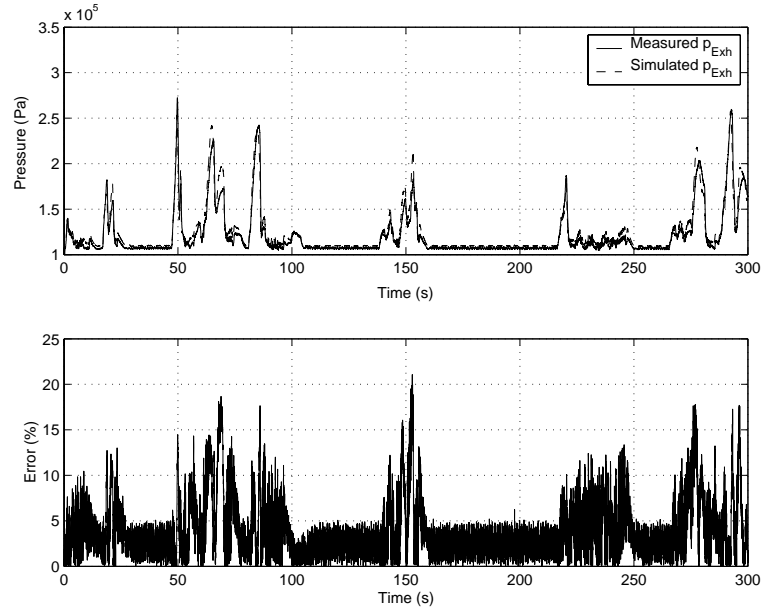
Figure 6.2: An example of how the model of p_{Exh} behaves compared to the measured value; Uphill driving.

pressure ratio over the turbine. It is called the original model. The second model was when ambient pressure was used directly. This is called the $p_{Turb} = p_{Amb}$ model. The third model was to use a static map (called the static map model) and the fourth model was a function of ambient pressure and a constant (called $p_{Turb} = f(p_{Amb})$). The results of the different models inserted in the turbine model are shown in Table 6.6

It can be seen in Table 6.6 that some of the models manage to get a lower mean- and RMS error than for measured values of p_{Turb} inserted in the model. They must thus compensate for some other error in the model. But no model manage to do this for the highway driving condition. The main difference of this measurement compared to the other is that it contains no idling speed. It has already been showed in Section 6.3.1 that the turbine model has an idling speed steady state error. The p_{Turb} models can compensate for that. Since the highway driving condition contains no idling speed, no compensation can be made. So to validate the p_{Turb} models only the highway driving condition will be considered.

The results show that just using p_{Amb} is not a sufficient model of p_{Turb}. The model that uses a static map on the other hand gives a little

p_{Turb} model	Pressure Errors (%)		
	e_{mean}	e_{RMS}	e_{max}
Mixed driving			
Measured p_{Turb}	3.86	5.16	25.08
Original model	3.66	4.97	27.55
$p_{Turb} = p_{Amb}$	4.39	5.65	28.07
Static table	4.09	5.35	26.20
$p_{Turb} = f(p_{Amb})$	3.47	4.81	27.28
Highway driving			
Measured p_{Turb}	3.07	3.95	20.45
Original	4.73	5.56	19.64
$p_{Turb} = p_{Amb}$	5.88	6.74	20.79
Static table	4.31	5.05	20.04
$p_{Turb} = f(p_{Amb})$	4.14	5.05	19.46
Uphill driving			
Measured p_{Turb}	4.08	5.34	23.09
Original	3.45	4.64	21.14
$p_{Turb} = p_{Amb}$	3.77	4.88	22.09
Static table	3.75	4.85	21.05
$p_{Turb} = f(p_{Amb})$	3.75	4.92	21.62

Table 6.6: Comparison of how the four different models of p_{Turb} affect exhaust manifold pressure.

better result but the main problem with this model is that it disables some of the diagnosis that the model is purposed for. Finally the last model that is a function of p_{Amb} and a constant gives the best results. This even though it cannot simulate the dynamics of the pressure after the turbine. Hence it can be confirmed that the effect of pressure after the turbine is important mainly at low pressure ratios over the turbine as stated in Section 4.4.1. It is decided to use this last model since it gives the best results and it doesn't disable any diagnosis operations.

6.4   EGR Model Validation

The overall model of the engine has been improved and the EGR system can now be included in the model.

6.4.1   EGR Mass-flow Model Validation

To validate the model of the mass-flow properly it would be necessary to measure the mass-flow through the EGR system. However, since

this is not possible some other, measurable, signal has to be used to make the validation. The closest signals are pressure and temperature in the intake manifold. This means, once again, that no proper validation looking at the actual errors in the mass-flow model can be made. It is only possible to say if the mass-flow model fits the intake manifold model. Measurement data with EGR turned on are used for validation. The inputs to the EGR model are exhaust pressure and exhaust temperature. Measured signals will be used as inputs to the EGR model, to see how only the EGR mass-flow model affects the intake manifold. Also measured T_{EGR} and T_{Wall} will be used so that focus is only on the mass-flow estimation in the EGR model.

A comparison is made, in Table 6.7, of intake manifold pressure and temperature for both EGR turned on and off. The values for EGR turned off are not exactly the same as in Table 6.1. The difference is because here, measured T_{Wall} is used instead of simulated. It is important to remember that this is thus a comparison between different simulation files. The measurements have been made driving the same cycle but e.g. the speed profile will not be exactly the same due to traffic etc.

EGR	Pressure Errors (%)			Temperature Errors (%)		
	e_{mean}	e_{RMS}	e_{max}	e_{mean}	e_{RMS}	e_{max}
Mixed driving						
On	1.84	2.53	15.52	7.95	9.46	23.92
Off	1.48	2.11	13.56	9.57	11.64	24.64
Highway driving						
On	2.02	2.65	10.23	6.24	7.06	17.88
Off	1.73	2.29	9.09	4.91	5.36	10.75
Uphill driving						
On	1.78	2.49	18.42	7.45	9.09	26.41
Off	1.27	1.91	13.16	16.14	17.10	27.05

Table 6.7: Intake manifold pressure- and temperature errors both with EGR turned on and off.

The introduction of EGR seems to affect all the pressure errors for all three driving conditions similarly. There seems to be about 0.3% increase in mean pressure error. This must be considered to be a very good result. The mean temperature error is radically affected only in the uphill driving condition. Overall the model seems to cope very well with the introduction of EGR gases, even though they have a much higher temperature and their temperature vary over a wider range.

The mean value model of the EGR valve could be sensitive to pulsations in the pressure ratio over the valve, as already mentioned in

Section 5.1. This would be significant only when the pressure ratio over the valve is close to unity. Then the mean value model estimates a very small, or zero mass-flow through the valve but in reality the pulsations could cause a mass-flow. Low pressure ratios over the EGR valve occurs at low power engine output, e.g. during idling speed. In the measurements used for validation, low pressure rations over the EGR valve are more common for mixed driving than for highway driving. Therefore, since measured inputs (that catches pulsations) to the EGR model are used in Table 6.7, the pulsations would cause the difference between when EGR is on and off to be larger for mixed driving than for highway driving. The difference is almost the same for the two driving conditions and the influence of pulsations will therefore be considered as neglectable. The reason could be that a compensation for pulsations were included in the identification of the EGR valve effective area table.

It would be interesting to also make a comparison with measurements made with the old EGR valve. Since the model is almost the same it could then be seen if there were any advantages of using the electrically controlled valve instead of the pneumatically controlled valve. However, the exhaust pressure sensor was broken when the measurements with the old valve were made. The sensor was replaced first after the change of the EGR valve. Also the intake manifold wall temperature sensor was installed after the change of EGR valve. So a comparison cannot be made here, it will instead be made in Section 6.5 where the EGR system model is run with simulated p_{Exh} and T_{Wall} as inputs.

6.4.2   EGR Temperature Model Validation

Validation of EGR temperature is fairly straight forward. It is possible to measure T_{EGR} so a direct comparison can be made. Still, measured p_{Exh} and T_{Wall} are used as inputs to the EGR system model. Table 6.8 show the errors for different driving conditions. Also an example is shown in Figure 6.3.

	Temperature Errors (%)		
	e_{mean}	e_{RMS}	e_{max}
Mixed driving	13.79	18.09	55.28
Highway driving	16.04	19.25	54.29
Uphill driving	15.69	20.16	52.35

Table 6.8: Errors in model of EGR temperature.

The model manages to capture most of the dynamics in the temperature but some clear errors cause a maximum error of over 50%.
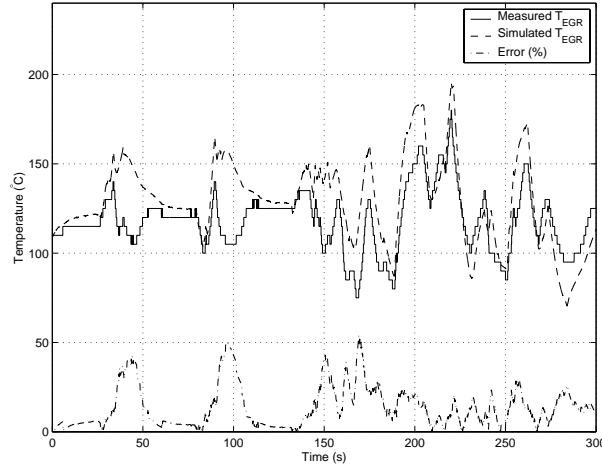
Figure 6.3: An example of how the model of T_{EGR} behaves compared to the measured value; Mixed driving.

This is a fairly good result considering that the temperature ranges over almost $100°C$.

It is also interesting to know how the errors in the T_{EGR} model affects the intake manifold pressure and temperature. The results of that are presented in Table 6.9. The errors in p_{Intake} and T_{Intake} are shown both for using measured and simulated T_{EGR}. Results are also shown for using a constant EGR temperature of $831K$. In this table the measured T_{Wall} is used as an input to the intake manifold model, so that focus is put only on how the EGR temperature model affects the intake manifold. In the EGR cooler model, on the other hand, simulated T_{Wall} will be used as input since it is the practical capabilities of the EGR temperature model that are interesting.

It is clear in Table 6.9 that the difference between using measured- and simulated EGR temperature in the intake manifold, is very small. The errors in T_{EGR} seem to compensate for some other error. That is why the results using simulated T_{EGR} give slightly better results than when for measured T_{EGR}. But the difference is very small and it can thus be said that the EGR temperature model is sufficiently good. It can also be seen in Table 6.9 that it is not sufficient to use only a constant EGR temperature. The latter does not seem to affect mean- and RMS pressure error too much, it is even decreased for the mixed driving condition. But maximum pressure error is increased. All errors in the the temperature model are severely increased. The model of the EGR temperature will be used since it proved to give sufficiently good

	Pressure Errors (%)			Temperature Errors (%)		
T_{EGR}	e_{mean}	e_{RMS}	e_{max}	e_{mean}	e_{RMS}	e_{max}
Mixed driving						
Measured	1.83	2.53	15.08	7.95	9.46	23.92
Simulated	1.81	2.50	15.14	8.08	9.70	23.87
Constant	1.77	2.61	23.52	50.77	60.73	141.88
Highway driving						
Measured	2.01	2.65	10.21	6.24	7.06	17.88
Simulated	2.01	2.63	10.16	5.90	6.76	17.37
Constant	2.20	3.11	16.14	11.36	18.89	77.97
Uphill driving						
Measured	1.77	2.48	18.36	7.45	9.10	26.42
Simulated	1.73	2.44	18.41	8.44	10.30	26.47
Constant	1.87	2.84	18.51	48.62	55.41	122.93

Table 6.9: Intake manifold pressure- and temperature errors with measured-, simulated and constant T_{EGR} as input to the model.

results.

6.5   Complete Model Validation

All the submodels have now been validated and the ones that gave best results have been picked. All those submodels have here been put together into one single model that will be validated against measurements. There will also be a comparison with measurements with the old EGR valve, simulated with the original EGR model, inserted in the new engine model, so a comparison with the new and the old EGR valves and their models can be made. The results are shown in Table 6.10.

The new model can simulate intake manifold pressure with a mean error under 3% and a maximum error around 20% when EGR is turned on. Even though this is more than double the mean pressure error when EGR is turned off, it must be considered as a good result. The temperature errors seem to have changed in the corresponding manner. Mean pressure error is increased more for mixed and uphill driving. The reason for this could be that for those driving conditions more EGR is used, since those measurements includes idling speed.

A comparison with Table 6.7, where only measured inputs to the EGR model are used, shows that the difference in mean pressure error is around 1%. It was shown in Table 6.9 and 6.3 that the errors in T_{EGR} and T_{Wall} signals, that also were measured inputs to the model

	Pressure Errors (%)			Temperature Errors (%)		
EGR	e_{mean}	e_{RMS}	e_{max}	e_{mean}	e_{RMS}	e_{max}
Mixed driving						
Off	1.52	2.13	12.32	7.19	9.17	22.75
New Valve	2.69	3.16	13.81	9.31	11.13	26.70
Old Valve	4.17	4.87	31.35	23.77	30.82	82.00
Highway driving						
Off	1.75	2.31	8.76	1.95	2.42	7.86
New Valve	2.15	2.91	11.84	5.17	6.50	21.42
Old Valve	2.32	3.24	32.74	8.35	13.18	66.68
Uphill driving						
Off	1.45	2.08	15.03	8.20	9.62	25.13
New Valve	2.76	3.34	18.27	12.26	14.02	33.60
Old Valve	4.47	5.26	18.60	26.40	35.24	84.16

Table 6.10: Intake manifold pressure- and temperature errors in the final model for different driving conditions. Validation for: No EGR, EGR on with the new EGR valve and also EGR on with the old EGR valve.

in Table 6.7, have very little influence on mean intake manifold pressure error. This means that most of the error increase when EGR is turned on, comes from the exhaust pressure and temperature model. It was concluded in Section 6.3.1 that the VNT actuator model causes an exhaust pressure steady state error. It could be this that causes most of the 1 % error increase. Table 6.10 shows larger mean pressure errors compared to no EGR measurements for measurements with idling speed (mixed and uphill driving conditions). It was during idling speed that the turbine model gave a steady state error. It will therefore be suggested, that to achieve even better results, it will be necessary to look at alternative solutions in the exhaust- and turbine models.

The old EGR valve (and belonging model) gives mean pressure errors under 5%, i.e. slightly worse than the new valve. Maximum pressure error has risen to over 30% and the temperature is very badly modeled which isn't very surprising since the old valve model uses constant EGR temperature. The model for the old valve has a different map for transforming EGR control signal into effective valve area than the one identified in this thesis. It has not been investigated further whether the difference in results are caused by the new valve, or because of a better EGR valve area map. It seems though, that the results are closer to those of the new EGR valve for driving conditions when there is no idling speed. The problems of the old valve could hence be limited to that operating point.

Finally the results of the complete new model and the complete original model will be compared. The results are shown in Table 6.11. The new model is shown to be superior for all types of errors. For pres-

	Pressure Errors (%)			Temperature Errors (%)		
Model	e_{mean}	e_{RMS}	e_{max}	e_{mean}	e_{RMS}	e_{max}
Mixed driving						
New Model	2.69	3.16	13.81	9.31	11.13	26.70
Old Model	5.65	9.17	34.28	96.74	123.32	387.75
Highway driving						
New Model	2.15	2.91	11.84	5.17	6.50	21.42
Old Model	4.80	7.00	36.23	34.18	65.11	351.32
Uphill driving						
New Model	2.76	3.34	18.27	12.26	14.02	33.60
Old Model	4.85	7.78	29.46	98.49	131.41	379.11

Table 6.11: Intake manifold pressure- and temperature errors in the final model for different driving conditions. Validation of the new model and the original model.

sure the errors have been halved and for temperature the improvement is even better. It is thus fair to say that the aim to improve the model has succeeded.

Chapter 7

Diagnosis

In this chapter the previously developed model will be used in a simple model based diagnostics system. Since this is the purpose of the model this can be seen as yet another way to validate the model. Diagnosis of only one type of fault will be considered: intake manifold leakage. The aim is to be able to detect the occurrence of a leakage in the intake manifold. The reason for choosing the intake manifold fault is, that work with this fault has been performed previously for this model, see [2]. The results with the new model can therefore be compared with the results presented there.

7.1 Introduction to Model Based Diagnosis

Model based diagnosis is based on having a process, in our case an engine, and also a model of that engine. The diagnosis is then made by comparing the model with the actual process. The model has been covered in the previous chapters. It is necessary to have a good model, since a comparison with the real process is made. The better the model is, the better the diagnostics system will perform. An overview of how a diagnosis system is set up is shown in Figure 7.1.

The diagnostics system is run on the same inputs as the engine. Also the outputs from the engine are inputs to the diagnostics system. From these inputs the diagnostics system then produces a statement, S, that tells if there is a fault or not and if so, which fault it is.

The statement is produced by comparing a test quantity, TQ, with a threshold, J. The test quantity is supposed to be something that can express the difference between the engine and its model. TQ should be small (ideally zero) when there is no fault in the engine and it should be large when a fault is present.
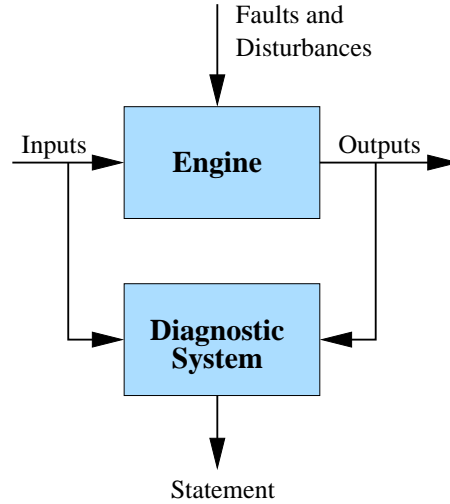
Figure 7.1: Overview of a diagnostics system.

Normally a diagnostics system handles many different faults. Each fault is then assigned to a fault mode. There is one mode for no fault, usually called NF, and one for each fault. Each fault mode has a model and its own test quantity. Structured hypothesis testing can then be used to isolate an occurring fault [15].

7.2   The Test Quantity and Threshold

A very simple diagnosis will be performed in this thesis. Only the NF fault mode will be considered. This means that a fault can only be detected, it can not be isolated. Since only intake manifold leakage is considered, it is assumed that there are no other faults in the system and isolation is therefore not necessary.

It is appropriate to create a test quantity by comparing measured and simulated intake manifold pressure. The test quantity is chosen in the same way as it has been done in [2], so a comparison can be made with the results presented there. The test quantity is:

$$TQ(t) = \frac{1}{t_1 - t_0} \cdot \int_{t_0}^{t_1} (p_{Intake}(t) - \hat{p}_{Intake}(t))^2 dt. \qquad (7.1)$$

where the interval $[t_0, t_1]$ was chosen to one minute. The difference $p_{Intake} - \hat{p}_{Intake}$ will be referred to as the residual.

The threshold J will be chosen manually. It has to be chosen carefully so that the diagnostics system not will give any false alarms but

still doesn't miss any faults.

60 minutes of measurements were made during highway driving, in order to set the value of the threshold, J. From these measurements 60 test quantities were calculated according to (7.1), one for each minute. From those test quantities a histogram was made, shown in Figure 7.2. The histogram shows that during 60 minutes of driving, no test quantity
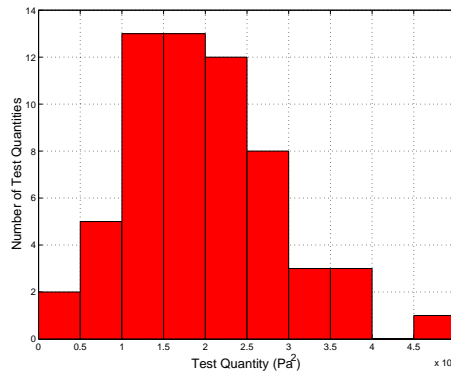
Figure 7.2: Histogram of 60 calculated test quantities when no leakage is present in the intake manifold.

exceeds $5 \cdot 10^7$, so if the threshold is set to $J = 5 \cdot 10^7$ it is not likely to be any false alarms. This is therefore the value used as threshold.

7.3 Results

In order to evaluate the diagnostics system on the model, measurements where a leakage is present in the intake manifold will be needed. A hole in the intake manifold has been drilled to accomplish this. In this hole special screws, drilled with different hole diameters can be fitted. To make a measurement, the screw with the requested hole diameter is fitted.

The measurements used to evaluate the diagnostics system are all made during highway driving. The reason for this is that mass-flow leakage out of a hole in the intake manifold is dependent on the pressure ratio over the hole. A large pressure ratio gives a large mass-flow and a small ratio a small or no mass-flow. It is the same relation as for e.g. the EGR valve in (5.1). The pressure outside the intake manifold will always be ambient pressure and it is known that during highway driving there are high pressures inside the intake manifold. Hence, highway driving measurements will be used because measurements show, that then there is a large pressure ratio over the hole in the intake manifold.

It is then possible to test the performance of the diagnostics system under good conditions.

Measurements were made, 15 minutes long, for each of the different hole diameters in the intake manifold. For these measurements, 15 test quantities were calculated according to (7.1), one for each minute. An example of this is shown in Figure 7.3. The measurement shown has been low-pass filtered. The rest of the measurements and their test quantities are shown plotted in Figure C.1 to C.4 in Appendix C. The results have been compiled in Table 7.1 along with the results of the old model (taken from [2]).
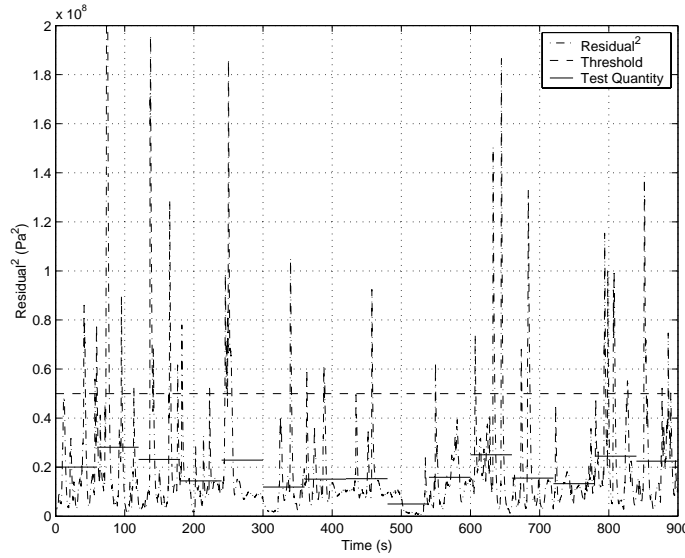
Figure 7.3: Test quantities calculated for 0 mm diameter hole in the intake manifold.

Leakage	Original	New Model	
Diameter	Model TQ	Max TQ	No. TQ over $J = 5 \cdot 10^7$
0 mm	$5.18 \cdot 10^7$	$2.81 \cdot 10^7$	0
2 mm	$1.51 \cdot 10^8$	$3.85 \cdot 10^7$	0
3 mm	$9.21 \cdot 10^8$	$5.22 \cdot 10^7$	1
4 mm	$5.23 \cdot 10^8$	$6.81 \cdot 10^7$	4
6 mm	$3.01 \cdot 10^9$	$1.87 \cdot 10^8$	11

Table 7.1: Test quantities for measurements with different hole diameters in the intake manifold.

The results show that with the new engine model it is barely possible to detect a 3 mm diameter hole. There is only one test quantity over the threshold for the 3 mm hole. The test quantity of the 3 mm hole is very close to the threshold and the conditions are very good so a real detection can be said to occur at the 4 mm hole, where there are four test quantities above the threshold.

A comparison of the results of the new and the old model in Table 7.1 shows, that there is an overall decrease in the value of the test quantity. The threshold for the old model was set to $7 \cdot 10^7$. This means that it was possible to detect the 2 mm diameter hole with the old model, according to the test quantity values shown in Table 7.1. But how can a model that has been shown to give worse results than the new model (see Section 6.5), give better diagnosis results? Well, one explanation could be that only one test quantity value for each hole size is presented for the original model. Having only one value to compare with doesn't say much of the actual behavior. Figure C.1 to C.4 (in Appendix C) show that the variance in the test quantity is quite large. This is why 15 different test quantities are calculated for each hole diameter in this thesis. It appears in [2] as if the test quantity values for the original model come from random one minute long measurements. If they were chosen randomly then the variance in test quantity value has not been considered and good results could be obtained simply by luck. A proper comparison is thus impossible.

Chapter 8

Summary, Conclusions and Extensions

8.1 Summary and Conclusions

An attempt has been made to reduce the overall error of a model of a turbocharged diesel engine, purposed for model based diagnosis.

Two previously implemented models for the intake manifold were compared. The model including heat transfer show best results. It has higher error peaks for pressure than the adiabatic model, but mean error is considered to be the most important error. The temperature on the wall of the intake manifold was modeled and parameters for the model were identified. The results of this proved to be satisfactory.

A comparison was made, using two different temperature sensors, to see if back-flow from the cylinders affects the temperature sensor in the intake manifold. The results show that the difference was very small. Using the temperature sensor in the intake manifold gives best results. That sensor was then used to create a volumetric efficiency map, with extra measurement points for low engine speeds. The results of this are very good.

A table that transforms VNT control signal into position of the nozzle lever was identified. The results of this are better than for the original model, where a linear function is used. The new model has a steady state error at idling speed. Different ways of modeling the pressure after the turbine were also evaluated. The best results are obtained by constructing a model as a function of ambient pressure and an identified parameter.

A model for the new EGR valve and its cooler were implemented and a table was identified. The results show that the EGR system, on its own, does not increase the errors too much. The exhaust system,

that produce the inputs for the EGR system, seems to be the cause of most of the errors. It is therefore suggested, as future extension, to consider alternative models of both the exhaust- and turbine systems, since the turbine model is one of the main influences on the exhaust system. Validation of the entire model shows, that the error almost is the double when EGR is turned on, compared to when EGR is turned off. This is still considered to be reasonably good results, since modeling of EGR is considered to be difficult. It was also shown that the old, pneumatically driven EGR valve, cause even larger errors. Hence, the change of the valve could be the main reason for the better results in the new model.

The final comparison between the original and the new model show that significantly better results have been obtained. The objective was to improve the original model and it can thus be said that the objective has been achieved.

Generally it can be concluded, that it is difficult to model an engine, since all relations are based on mass-flow and the mass-flow is not measurable without disturbing the system. This is considered to be the largest difficulty in this thesis. Some identifications in this thesis are made by estimating mass-flow from pressure and temperature sensors. This adds errors in the mass-flow model to the result, and the identification thereby compensates for errors in the mass-flow model.

Finally, the new model was tested in a simple diagnostics system for intake manifold leakage. It was shown that a 4 mm diameter hole in the intake manifold could be detected under good conditions.

8.2   Summarized Identification Procedure

The procedure in which identifications have been made in the model can be reviewed in the following manner:

Intake Manifold Wall Temperature:
- EGR: On/Off.
- Sensor Inputs: T_{Wall}, T_{Amb} and T_{Oil}.
- Method: Least-square fit of parameters.

Volumetric Efficiency:
- EGR: Off.
- Sensor Inputs: W_{Inter}, N_{Eng}, p_{Intake} and T_{Intake}.
- Method: Manual pick of measurement points at different static engine operation points.

Pressure after Turbine:
- EGR: On.
- Sensor Inputs: p_{Turb} and p_{Amb}.
- Method: Mean value during static idling speed.

VNT Actuator:
- EGR: Off.
- Sensor Inputs: X_{VNT}, T_{Exh}, p_{Exh} and p_{Turb}.
- Estimated Inputs: W_{Exh} estimated from X_{Inj}, N_{Eng} and W_{Inter} sensors.
- Method: Least-square fit of polynomial for selected parts (excluding parts where $\frac{p_{Exh}}{p_{Turb}} \to 1$) of mixed driving measurement.

EGR Valve:
- EGR: On.
- Sensor Inputs: X_{EGRV}, T_{Exh}, p_{Exh} and p_{Intake}.
- Estimated Inputs: W_{EGR} estimated from p_{Intake}, T_{Intake}, W_{Inter}, T_{Inter}, T_{Exh} and T_{Wall} sensors.
- Method: Least-square fit of polynomial for 10 minutes long mixed driving measurement.

8.3 Extensions

Possible topics for future work with this engine model are suggested in this section.

Exhaust manifold model: The exhaust manifold model seems to be the main reason for the errors when EGR is turned on. It could be investigated how a change of exhaust manifold state would affect the errors. It would be appropriate to evaluate having pressure as state, since this is the input to both the turbine- and the EGR model. It would perhaps be necessary to increase the number of states or to include heat transfer in the model.

Turbo model: The turbo model has a great influence on the exhaust manifold model. Perhaps it will be necessary to look at alternative ways of modeling the turbine, to achieve better results in the exhaust manifold.

References

[1] F. Karlsson. Modelling the intake manifold dynamics in a diesel engine, 2001. Master's Thesis, Linköpings Universitet, Linköping, Sweden.

[2] M. Butschek. Modeling and diagnosis of leakages in the air intake path of an automotive diesel engine. Master's Thesis, Fachhochschule Trier, Trier, Germany, 2000.

[3] M. Nyberg, T. Stutte, and V. Wilhelmi. Model based diagnosis of the air path of an automotive diesel engine. IFAC Workshop: Advances in Automotive Control, Karlsruhe, Germany, March 2001.

[4] World Wide Web, `http://www.daimlerchrysler.com`. Information about Daimler Chrysler AG.

[5] J.B. Heywood. *Internal Combustion Engine Fundamentals.* Automotive Technology Series. McGraw-Hill, Singapore, 1988.

[6] N. Watson and M. S. Janota. *Turbocharging the Internal Combustion Engine.* MacMillan Press Ltd, London, Great Britain, 1982.

[7] L. Nielsen and L. Eriksson. Course material vehicular systems. Linköpings Universitet, ISY, Vehicular Systems, Linköping, Sweden, 1999.

[8] R. Klingmann, W. Fick, H. Brueggemann, D. Naber, K.H. Hoffmann, and A. Peters. Die neuen common-rail dieselmotoren mit direkteinspritzung in der modellgepflegten e-klasse. *Motortechnische Zeitung, MTZ*, 7,8,9, Germany, 1999.

[9] World Wide Web, `http://www.etas.de`. Information about ETAS GmbH.

[10] D.T. Sandwell. Biharmonic spline interpolation of geos-3 and seasat altimeter data. Geophysical Research Letters, 2, 139-142, 1987.

[11] Y. Nakayama and R.F. Boucher. *Introduction to Fluid Mechanics.* Arnold, London, Great Britain, 1999.

[12] P.E. Moraal A.G. Stefanopoulou M. Jankovic M.J. van Nieuwstadt, I.V. Kolmanovsky. Experimental comparison of egr-vgt control schemes for a high speed diesel engine. Control System Magazine, Vol 20, no. 3, pp 63-79, 2000.

[13] L. Guzzella and A: Amstutz. Control of diesel engines. IEEE Control Systems Magazine, Vol 8, no. 9, Oktober, pp 53-71, 1998.

[14] A. Schlosser. *Modellbildung und Simulation zur Ladedruck- und Abgasrueckfuehrregelung an einem Dieselmotor.* VDI-Verlag, Aachen, Germany, 2000.

[15] M. Nyberg and E. Frisk. Diagnosis and supervision of technical processes. Course Material Diagnosis and Supervision, Linköpings Universitet, ISY, Vehicular Systems, Linköping, Sweden, 2000.

Appendix A

Validation Measurements Profiles

Engine speed and fuel injection profile of all files used for validation in this thesis are shown in this appendix. The measurements are sorted after their EGR setting.
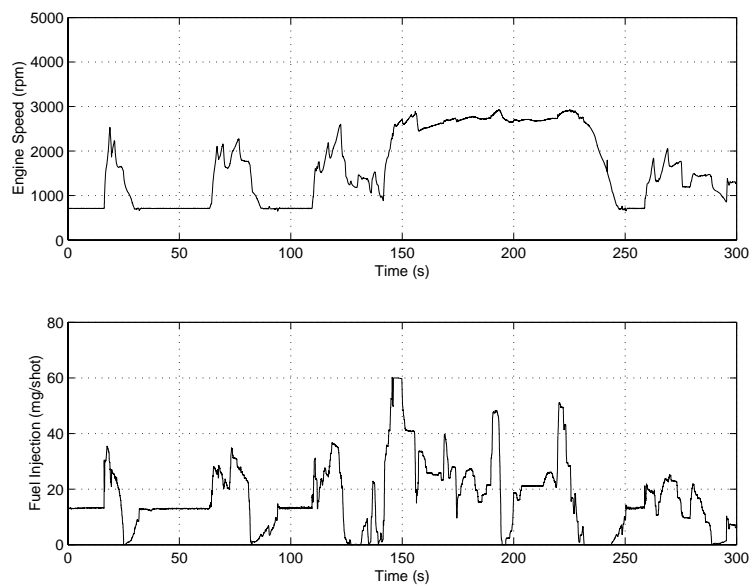
Figure A.1: Engine speed and fuel injection profile for mixed driving with EGR turned off.
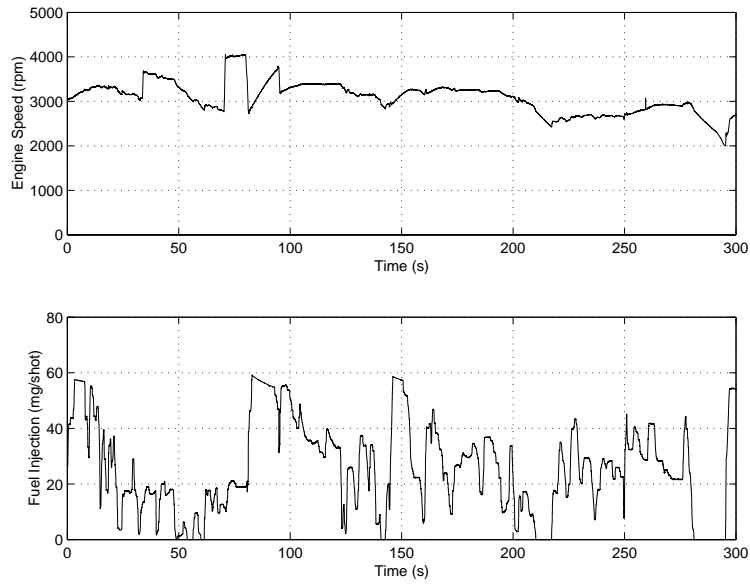
Figure A.2: Engine speed and fuel injection profile for highway driving with EGR turned off.
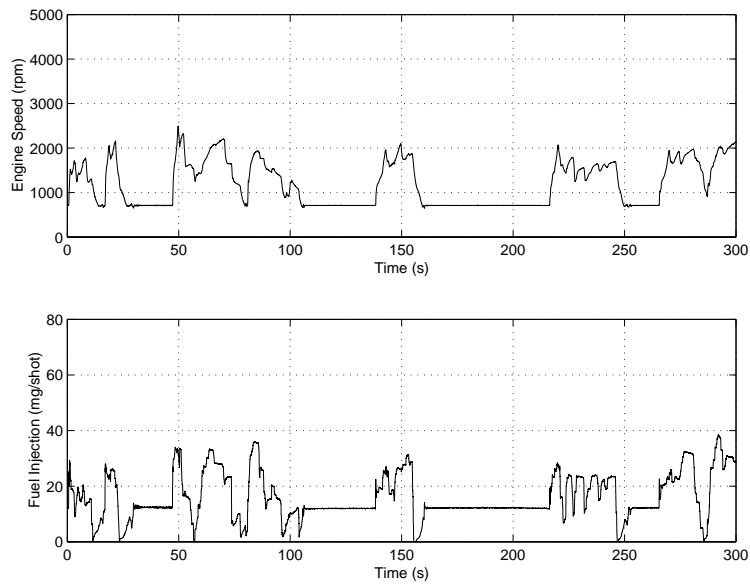
Figure A.3: Engine speed and fuel injection profile for uphill driving with EGR turned off.
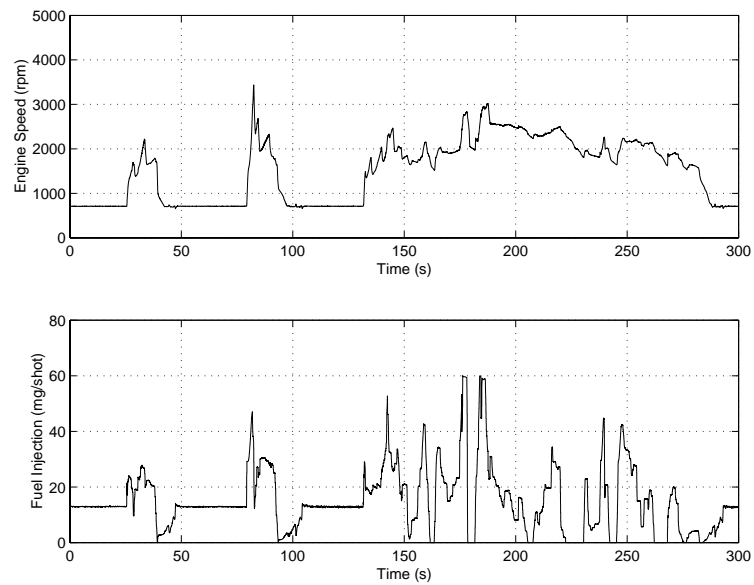
Figure A.4: Engine speed and fuel injection profile for mixed driving with EGR turned on and new EGR valve.
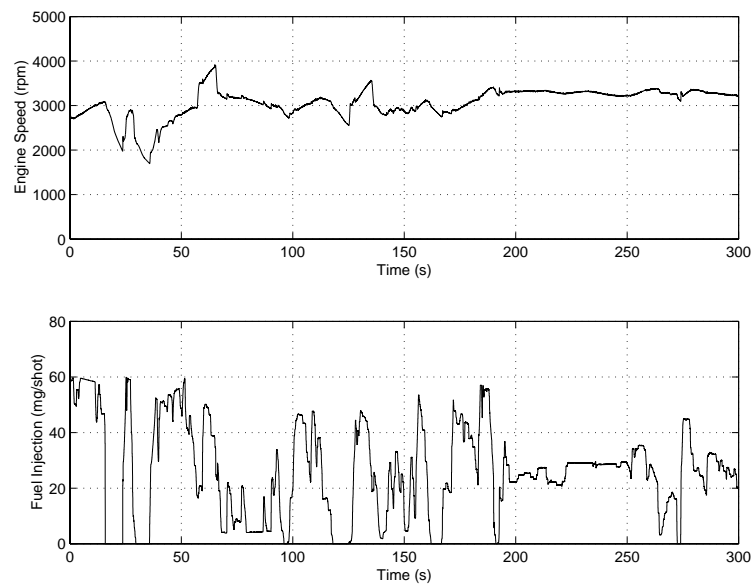
Figure A.5: Engine speed and fuel injection profile for highway driving with EGR turned on and new EGR valve.
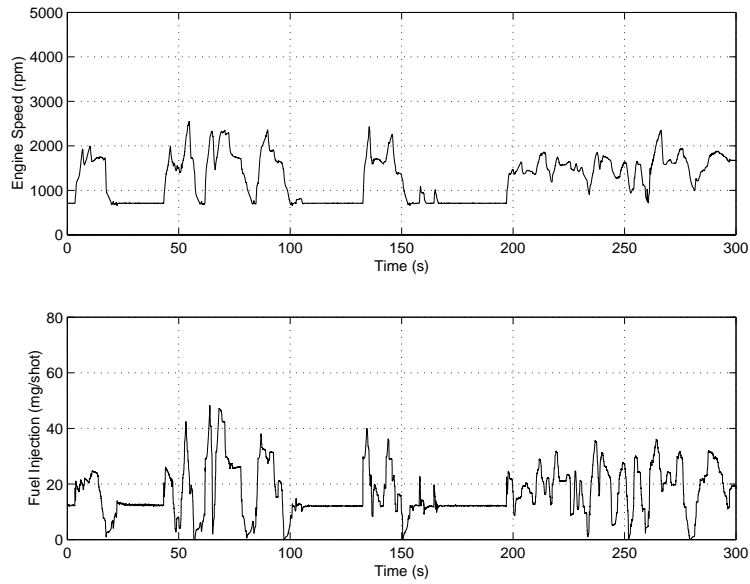
Figure A.6: Engine speed and fuel injection profile for uphill driving with EGR turned on and new EGR valve.
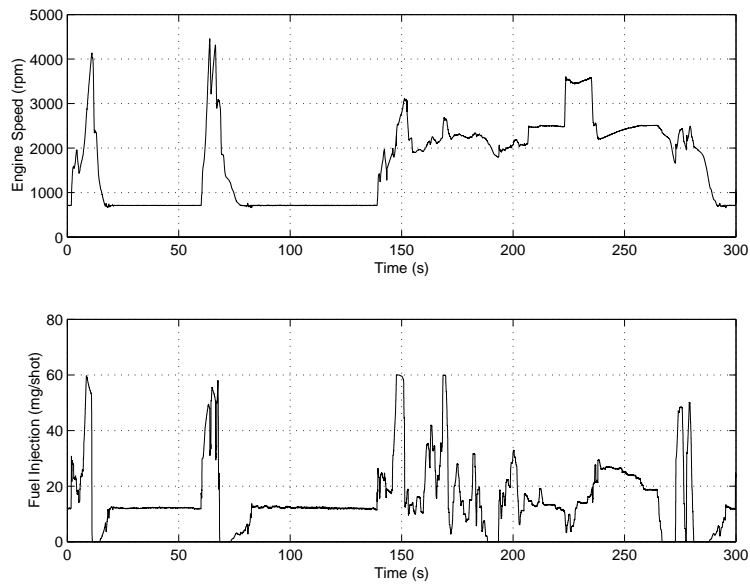
Figure A.7: Engine speed and fuel injection profile for mixed driving with EGR turned on and old EGR valve.
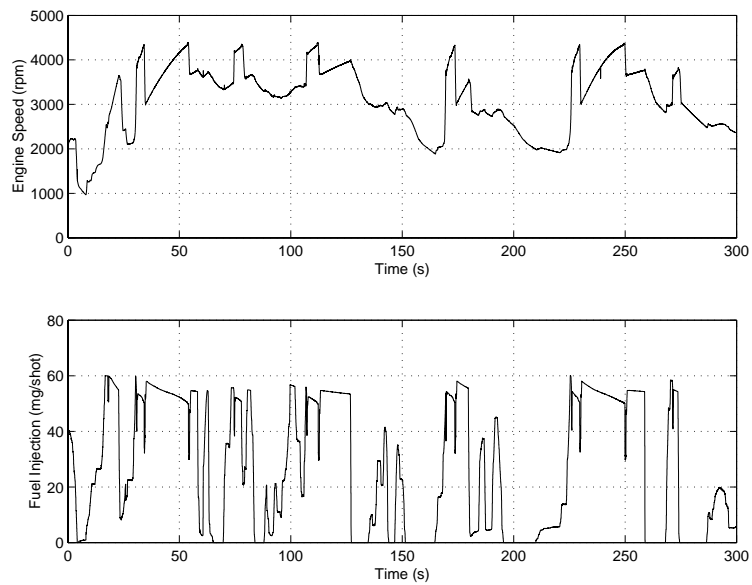
Figure A.8: Engine speed and fuel injection profile for highway driving with EGR turned on and old EGR valve.
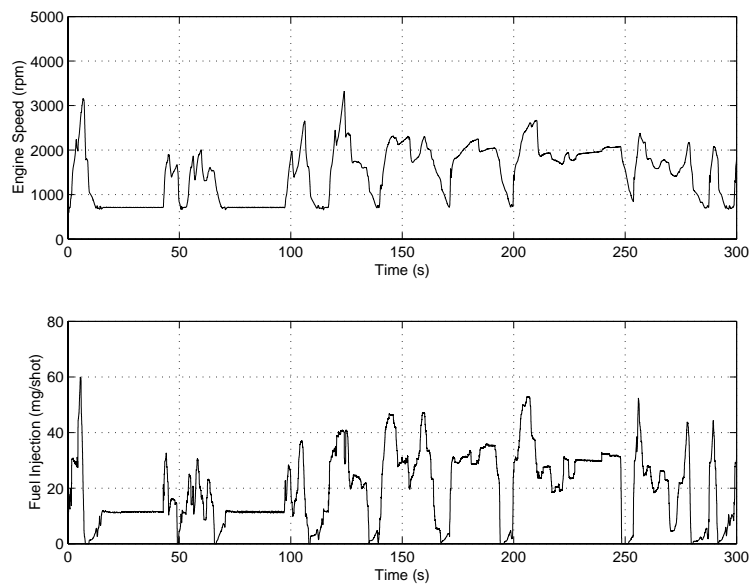
Figure A.9: Engine speed and fuel injection profile for uphill driving with EGR turned on and old EGR valve.

Appendix B

Validation Plots

In this appendix are validation plots shown. Plots are shown for complete model validation with; no egr, new egr valve and old egr valve.
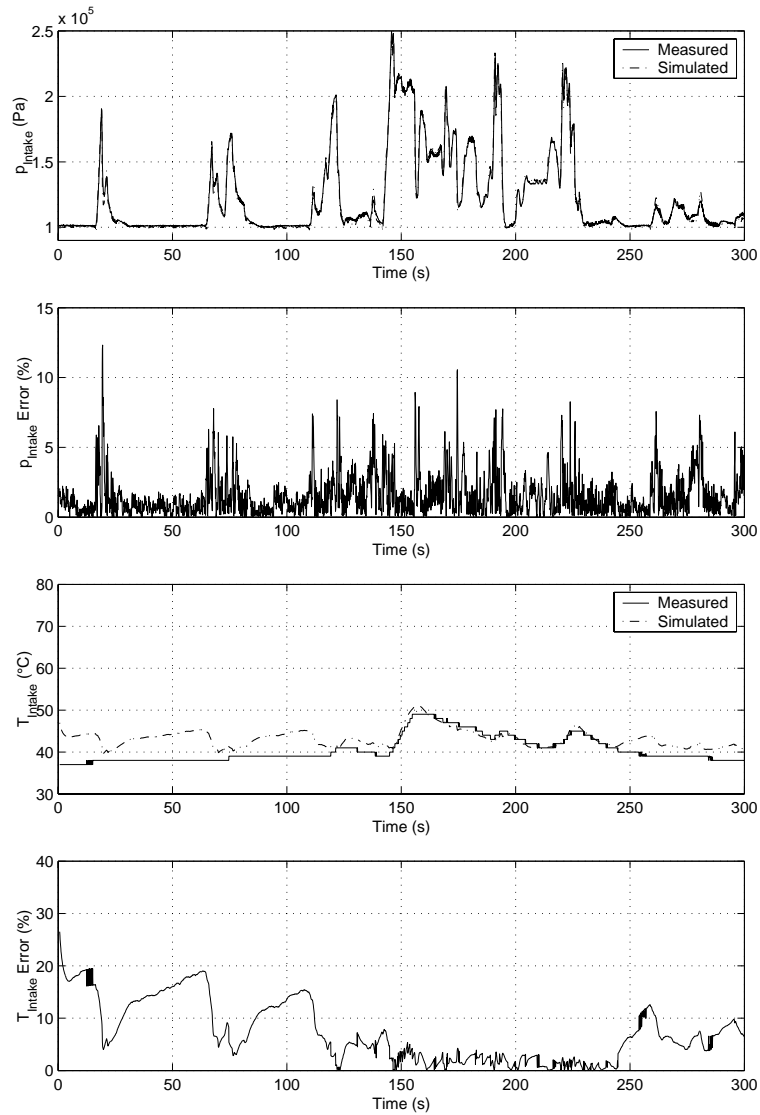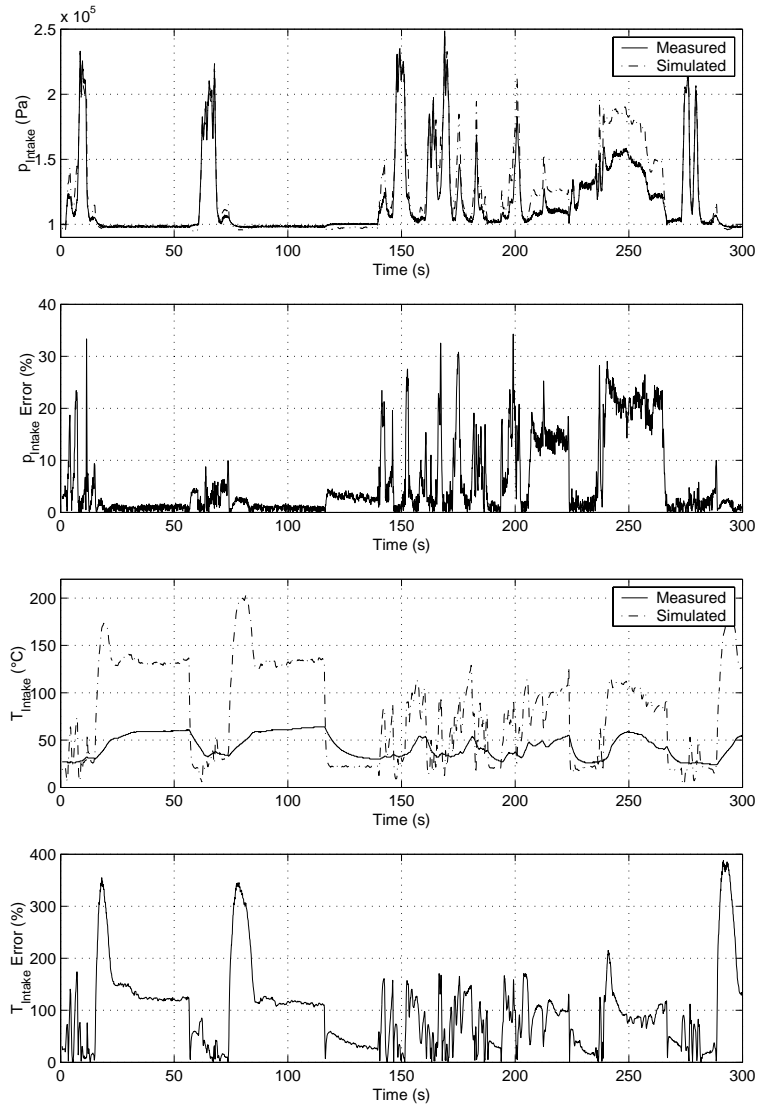
Figure B.1: Plots of Intake manifold pressure and temperature along with their errors for the complete model validation. Mixed driving with EGR turned off.
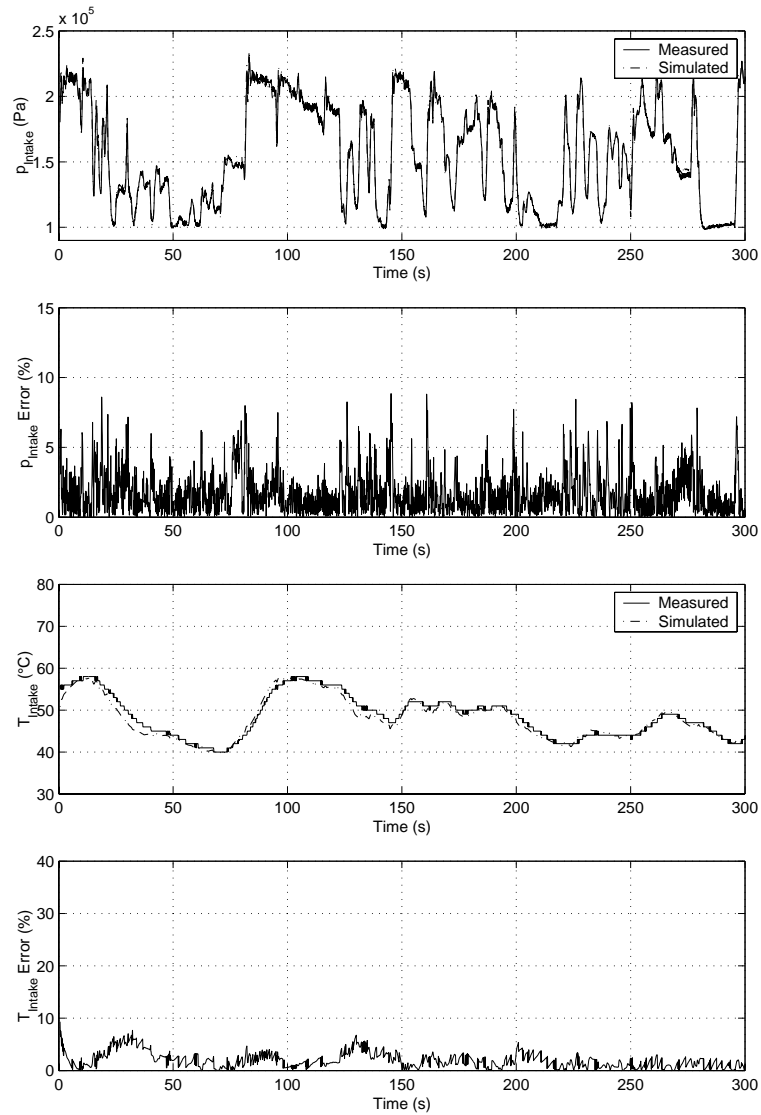
Figure B.2: Plots of Intake manifold pressure and temperature along with their errors for the complete model validation. Highway driving with EGR turned off.
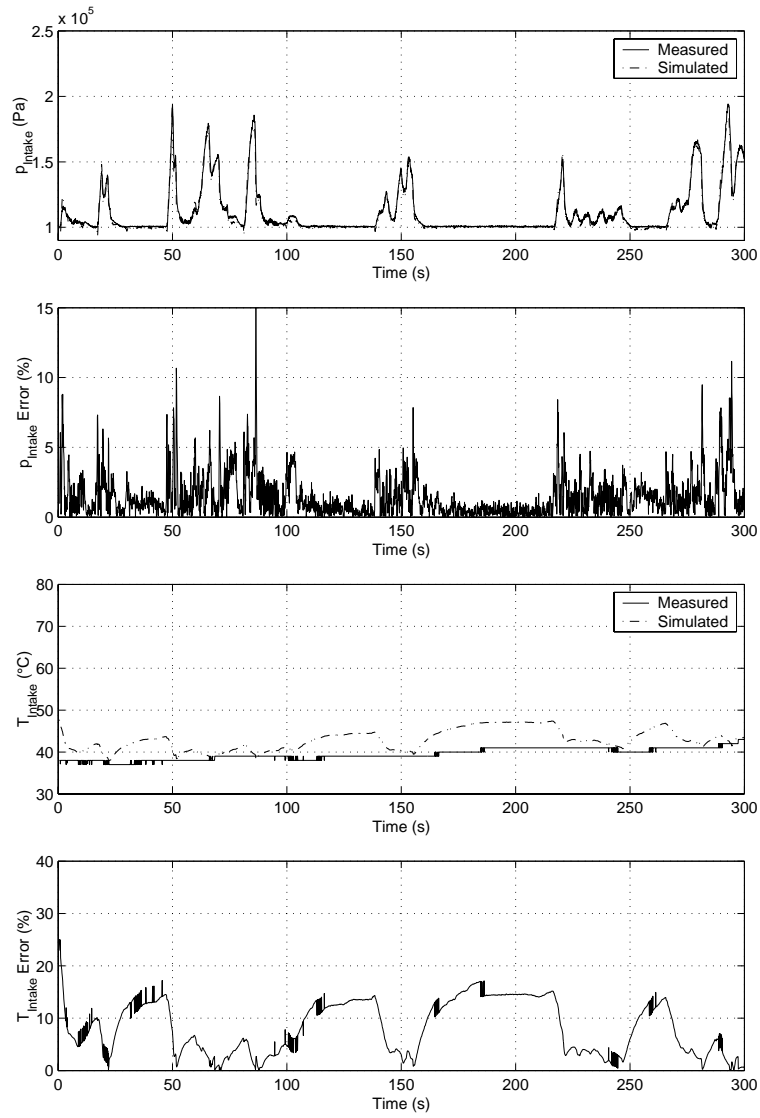
Figure B.3: Plots of Intake manifold pressure and temperature along with their errors for the complete model validation. Uphill driving with EGR turned off.
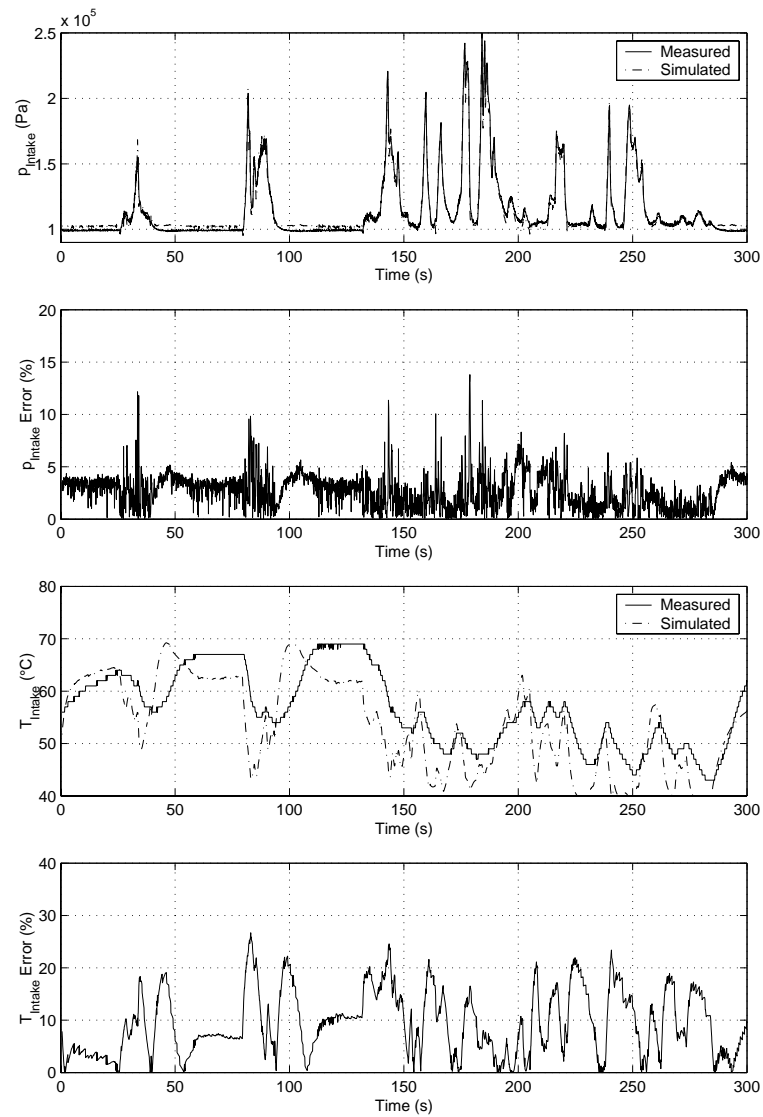
Figure B.4: Plots of Intake manifold pressure and temperature along with their errors for the complete model validation. Mixed driving with new EGR valve turned on.
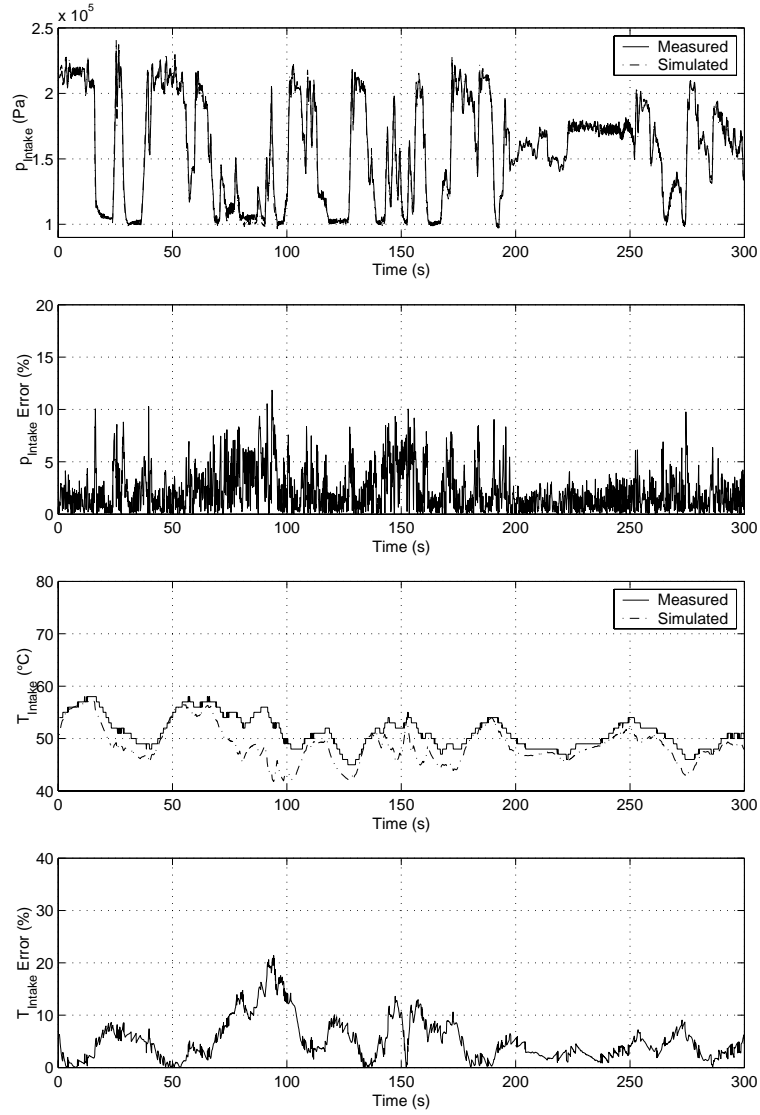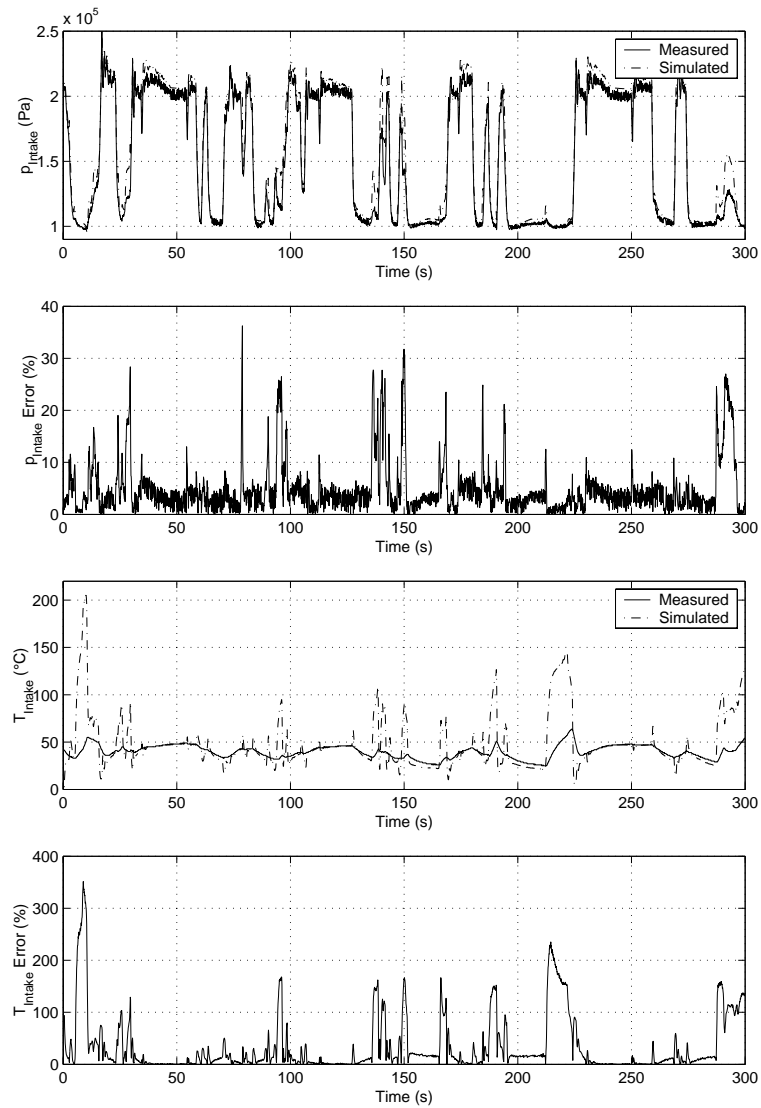
Figure B.5: Plots of Intake manifold pressure and temperature along with their errors for the complete model validation. Highway driving with new EGR valve turned on.
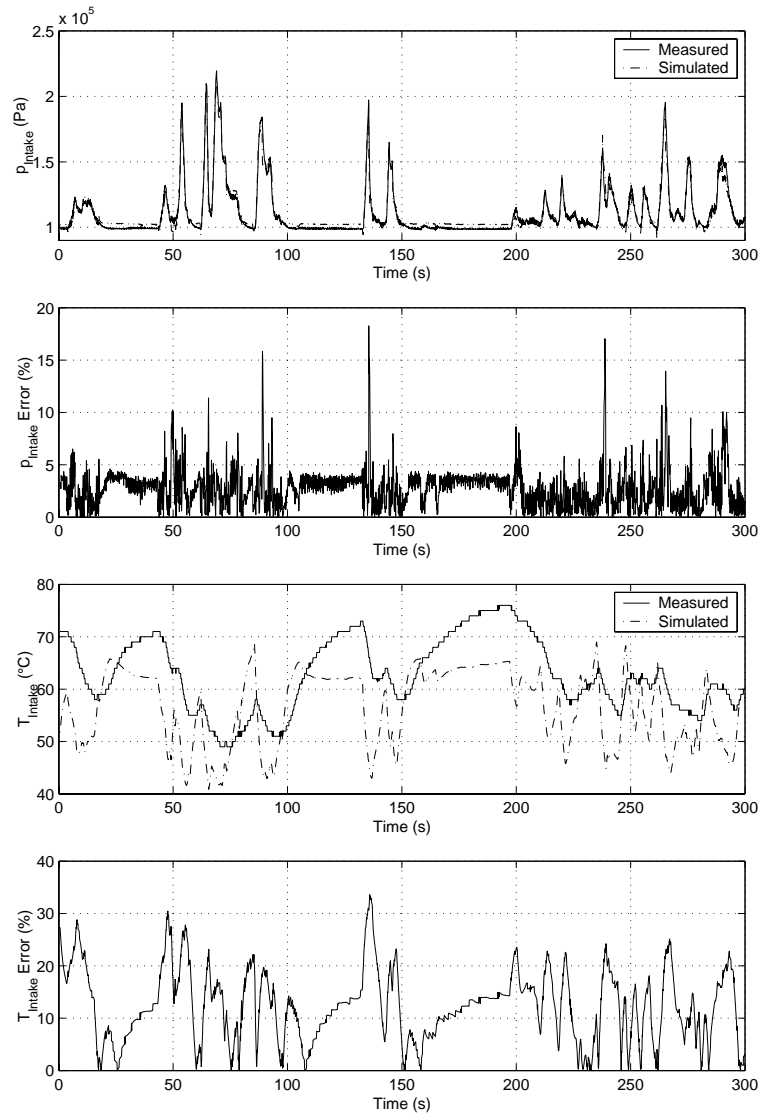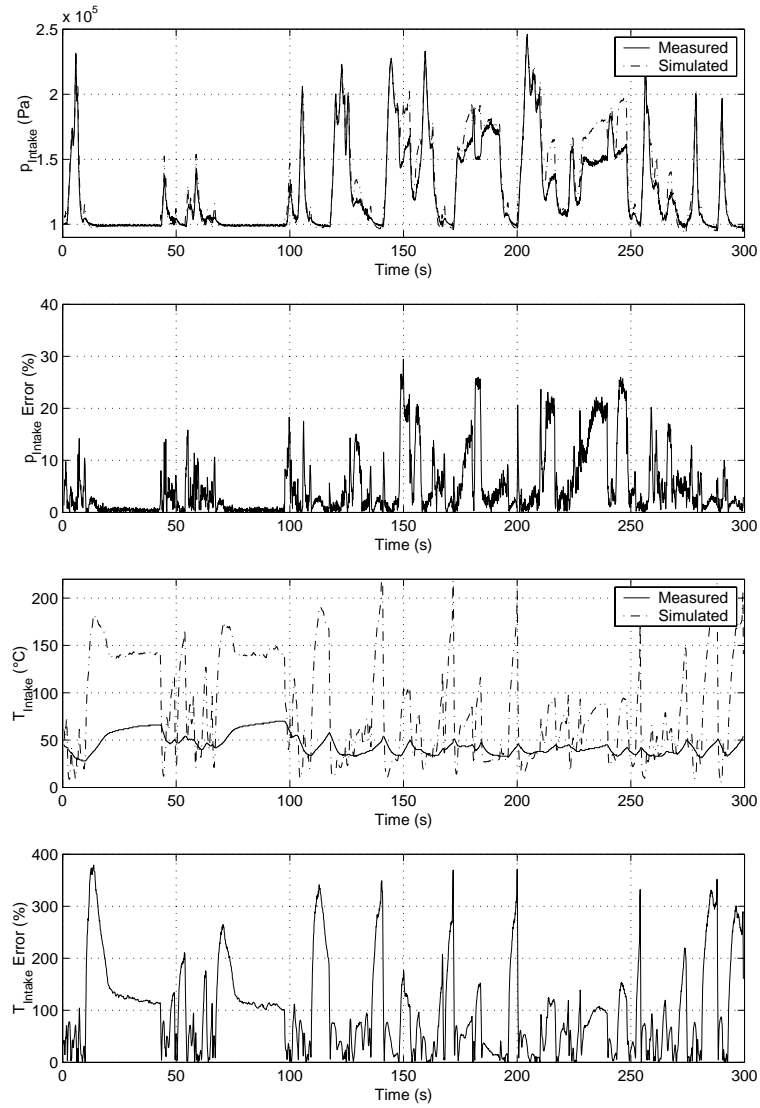
Figure B.6: Plots of Intake manifold pressure and temperature along with their errors for the complete model validation. Uphill driving with new EGR valve turned on.

Figure B.7: Plots of Intake manifold pressure and temperature along with their errors for the complete model validation. Mixed driving with old EGR valve turned on.

Figure B.8: Plots of Intake manifold pressure and temperature along with their errors for the complete model validation. Highway driving with old EGR valve turned on.

Figure B.9: Plots of Intake manifold pressure and temperature along with their errors for the complete model validation. Uphill driving with old EGR valve turned on.

Appendix C

Diagnosis Plots

This appendix shows test quantities calculated for different holes in the intake manifold.
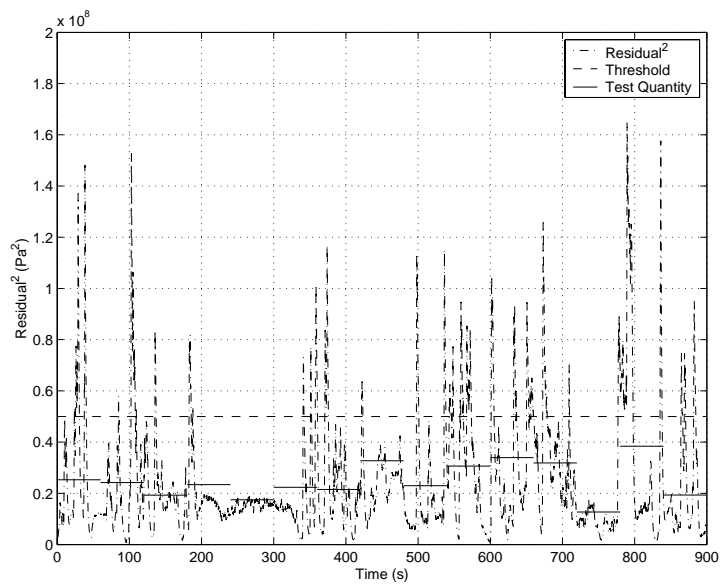
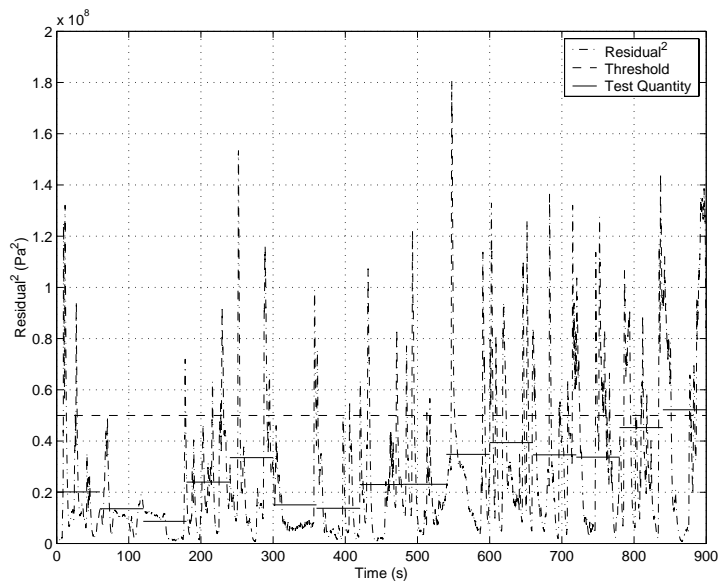Figure C.1: Test quantities calculated for 2 mm diameter hole in the intake manifold.

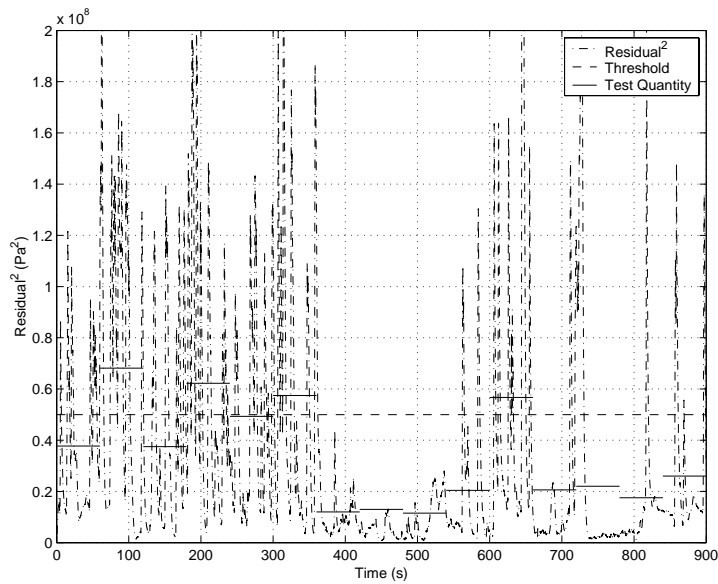Figure C.2: Test quantities calculated for 3 mm diameter hole in the intake manifold.

Figure C.3: Test quantities calculated for 4 mm diameter hole in the intake manifold.
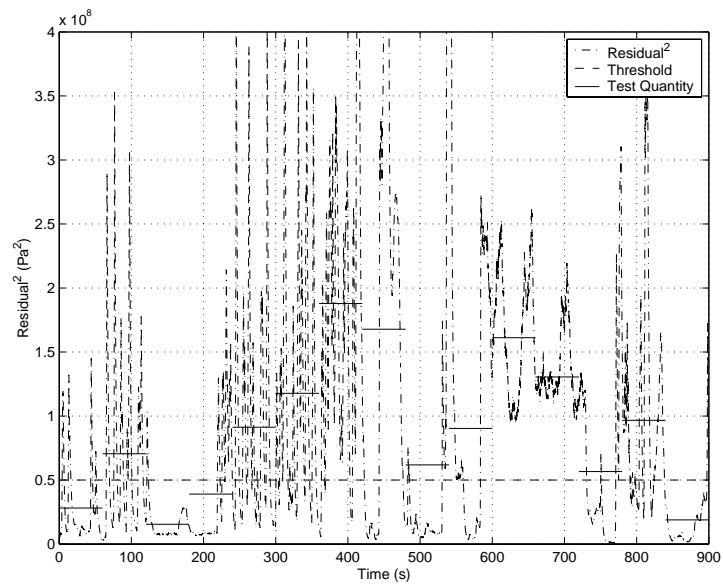
Figure C.4: Test quantities calculated for 6 mm diameter hole in the intake manifold.